



A G H

AKADEMIA GÓRNICZO-HUTNICZA IM. STANISŁAWA STASZICA W KRAKOWIE

WYDZIAŁ INFORMATYKI, ELEKTRONIKI I TELEKOMUNIKACJI

INSTYTUT ELEKTRONIKI

Praca dyplomowa

Scalable antenna arrays operating in broad frequency range featuring constant radiation pattern.

Skalowalne układy antenowe pracujące w szerokim zakresie częstotliwości o stałej charakterystyce promieniowania.

Autorzy:

Andrzej Kazimierz Dudek, Piotr Kanios

Kierunek studiów:

Elektronika i Telekomunikacja

Opiekun pracy:

prof. dr hab. inż. Krzysztof Wincza

Kraków, 2022

Contents

1. Introduction.....	7
1.1. Purpose and scope of this work	9
1.2. Authors' contributions	9
2. Antenna array theory	11
2.1. Extended array factor model	12
2.2. Scalable antenna arrays theoretical analysis and the virtual radiating element model.....	14
3. Multibeam scalable antenna arrays	21
3.1. Radiating element.....	21
3.2. Directional filter.....	25
3.3. T-junction power divider	30
3.4. Four-beam antennas.....	32
3.4.1. 8-element array	32
3.4.2. 12-element array	36
3.5. Three-beam antennas	42
3.5.1. 5-element array	42
3.5.2. 8-element array	45
3.5.3. 12-element array	48
4. Broadside beam scalable antenna array	53
4.1. Concept of a broadside beam scalable antenna array	53
4.2. Directional filter.....	59
4.3. Power dividers	62
4.4. Radiating elements	66
4.5. Measured results.....	71
5. Conclusions.....	73

1. Introduction

In recent years, due to the developments in modern wireless systems, the need for broadband antennas and antenna arrays has arisen. Since broadband radiating elements are well known [1] and relatively easy to design, the research caused by the demand for broadband systems led to the improvement of their properties [2] and the development of broadband feeding networks [3], [4]. However, it is worth underlining that the advancements concerning single antenna elements that led to the extending of operational bandwidth are crucial in the antenna arrays development. It is caused by the fact that the antenna array is composed of single radiating elements spaced in a proper way [5]. In order to achieve array's broad operational bandwidth it is necessary that the array consists of broadband radiating elements. Moreover, the antenna arrays were thoroughly researched and their broadband properties were investigated. The investigation showed that the broadband antenna arrays have problem with keeping radiation pattern characteristics, such as half-power beamwidth (HPBW) and beam direction, constant throughout operational frequency range as it is seen in [3] or in [6]. In order to prevent changes in the aforementioned characteristics the scalable antenna arrays were introduced [7] because they allow for maintaining constant HPBW and beam direction.

Since the introduction of scalable antenna arrays, numerous design concepts have been developed. In [7], a dual-band multibeam antenna array fed by a modified 4×4 Butler Matrix has been proposed. That approach allows for achieving two sets of 2 beams that have orthogonal polarizations and are pointing at 2 different directions at low frequency, whereas at high frequency 4 independent beams pointing at 4 different directions are obtained. However, that concept is not fully scalable because it ensures operation in only two bands located around the low frequency and high frequency instead of the entire frequency range between the aforementioned low and high frequencies. In [8] broadband radiating elements were utilized and uniformly spaced. Moreover, the frequency-selective feeding network, based on balanced directional filters, that gradually switches the signal between radiating elements, was used. That approach allows for obtaining constant beam direction and HPBW in the one-octave frequency range however it can be used only for antenna arrays consisting of an odd number of broadband radiating elements. Subsequent research has shown that it is possible to realise scalable antenna arrays having even number of radiating elements [9]. For switching purposes a frequency-selective feeding network based on an unbalanced directional filter was proposed. In both concepts two types of elements can be distinguished. The first type of elements are the elements between which RF power is switched depending on frequency.

On the other hand there are elements which are fed with constant RF power throughout the entire operational frequency range. Furthermore, novel variations of frequency-selective feeding networks were investigated along with antenna arrays having an operational frequency range greater than one frequency octave. In [10] and [11] frequency-dependent diplexers are utilized. Moreover, the antenna arrays' operational frequency ranges are 3:1 and 2.6:1, respectively.

Every approach presented in [8]-[11] is characterized by utilization of a frequency-selective feeding network that gradually switches the RF power between the elements and ensures near 0° phase progression between its outputs. It means that the aforementioned scalable antenna arrays have broadside radiation pattern (beam is directed at 0°). To utilize multibeam antenna arrays it is necessary to provide nonzero phase progression between the elements of an antenna array. Such phase progression between the radiating elements allows them to produce a beam that have a slanted angle. In order to develop multibeam scalable antenna arrays it was required to design such feeding networks that ensure both appropriate signal switching and proper phase shift between the outputs. First approaches to the design of multibeam scalable antenna arrays utilized modified Butler matrices [12] that change their behaviour throughout operational frequency range. Further research showed that by the application of modified Butler matrices it is possible to extend the operational frequency range of the antenna array from 2:1 in [12] to 3:1 in [13]. The modified Butler matrix design complexity led to the development of a less complex feeding network based on directional filters [14]. It is worth underlining that the approaches presented in [13] and [14] allow realisation of only two-beam scalable antenna arrays and cannot be used to develop antenna array having a greater number of beams.

The design process of multibeam scalable antenna arrays is more complex than the design process of broadside scalable antenna arrays. Not only they need more complex feeding networks ensuring both proper phase progression between array elements and appropriate signal switching, but also they require befitting radiating elements. In broadside antenna arrays more directive radiating elements having relatively smaller HPBW can be used. Whereas, in multibeam antenna arrays radiating elements with greater HPBW are desired to ensure proper array operation. It results from the fact that the radiation pattern of an array is a product of the array factor (AF) and the radiation pattern of elements utilized in the array. In most cases the maximum of the element radiation pattern is at 0° which corresponds to the maximum of AF having 0° phase progression between array elements (broadside beam). At more tilted angles the directivity of the radiating element is lower and this way the sidelobes present in AF can be attenuated while the main beam is not. On the other hand, when the phase progression is nonzero the main beam in AF is pointing at different direction than 0° . In this case the main beam is attenuated and the side-lobe level rises. Moreover, with the frequency increase the ratio of constant radiating element aperture and the wavelength rises and that has impact on the element's radiation pattern causing an increase in directivity and therefore a decrease in HPBW. From the aforementioned facts it follows that radiating elements utilized in multibeam scalable antenna arrays should have low directivity and therefore great HPBW. Moreover, the directivity variation with the frequency increase should be minimized in order to ensure satisfactory array radiation patterns.

1.1. Purpose and scope of this work

The purpose of this thesis is to gather and present authors' research regarding both multibeam and broadside beam scalable antenna arrays. In this work, novel concepts for development of scalable antenna arrays are analyzed theoretically. For theoretical analysis a novel model of virtual radiating element is shown. Moreover, all concepts were manufactured and verified by measurements of the proposed antenna arrays. Results of these measurements are reported in this thesis. It is worth underlining that this thesis is based on authors' scientific articles and conference papers. First, parts of this work are based on a published article [15]. Moreover, authors of this thesis authored and coauthored the following conference papers [16] and [17] which are also presented in this work. Lastly, parts of this work were created on the basis of an article under review [18].

This thesis is organised as follows. In Chapter 2, the theoretical models are profoundly discussed. In Chapter 3, concepts for realisation of multibeam scalable antenna arrays are presented. Besides the concepts, the development process is shown including radiating element and feeding network design, their simulation results and the results obtained during measurements. Similarly, broadside beam scalable antenna array is discussed in Chapter 4. The thesis ends with conclusions in Chapter 5.

1.2. Authors' contributions

Authors contributed to this work equally. Andrzej Dudek was responsible for the following parts i.e., theoretical analysis of the scalable antenna arrays, development of the model of virtual radiating element, and development of figures presented in this work. Moreover, he designed, manufactured and measured directional filters utilized in the feeding networks. Piotr Kanios was responsible for the following parts i.e., development of all radiating elements, electromagnetic simulations of all scalable antenna arrays, and development of power dividers. Furthermore, he manufactured and measured all of the radiating elements and power dividers. Measurements of all scalable antenna arrays were conducted by both authors. Andrzej Dudek is the author of Chapters 2 and 4 apart from the Sections 4.3 and 4.4 which were written by Piotr Kanios. Piotr Kanios is the author of Chapter 3 apart from the Section 3.2 and Subsection 3.5.2 which were authored by Andrzej Dudek. Chapters 1 and 5 are jointly written by Andrzej Dudek and Piotr Kanios.

2. Antenna array theory

Theoretical radiation pattern of the antenna array can be described by its array factor (AF) [5]. The AF is a mathematical model in which N ideal radiating elements in receiving mode are assumed. Such elements have ideal omnidirectional radiation pattern and do not have size, so they are considered as points. These points are placed along the axis. The receiving mode is assumed for analysis simplicity since it is well known that passive antennas have the same radiation pattern in both receiving and transmitting mode so the obtained AF is common for both operation modes. Furthermore, for each possible direction a plane wave is received by the radiating elements in such a way that the signal received by the whole antenna array is a superposition of signals received by individual elements. Moreover, the interactions between elements, which occur in reality and affect the received signal like e.g. mutual coupling, are ignored. That mathematical model and its graphical explanation are shown in equation 2.1 and in Fig. 2.1, respectively.

$$AF(\Theta, f, \bar{x}) = \sum_{i=1}^N \exp(j \frac{2\pi f}{c} x_i \cos \Theta) \quad (2.1)$$

where

Θ – incident plane wave angle,

f – the signal frequency,

\bar{x} – N -element vector containing positions of radiating elements,

c – the speed of light,

x_i – the i -th element of radiating elements position vector \bar{x} .

The model shown in equation 2.1 is the most simplistic model of the antenna array AF. Firstly, it is worth to consider the radiating elements positioning and the frequency f at which the array operates. Then the incident plane wave angle Θ is analyzed. The positions in which radiating elements are placed are closely related to the frequency of operation. Moreover, their positions are fixed but can be optimized to achieve the desired radiation pattern. In most cases the optimal distance between adjacent elements has to be kept around half a wavelength $\lambda/2$ at the frequency of operation. Therefore, if the frequency increases the wavelength decreases. That leads to the observation that since the distance between elements is constant the relative distance between elements increases. That dependency affects the AF. One of the observed changes is the decrease in HPBW.

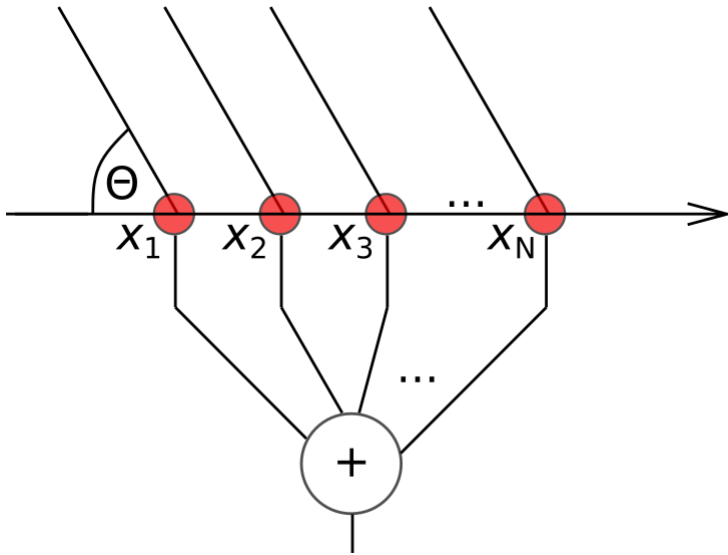


Fig. 2.1. Graphical explanation of simple AF model shown in equation 2.1.

For fixed frequency and radiating elements positions the incident plane wave angle Θ is the parameter that allows to analyze in which direction the array radiates the power. As it was mentioned for simplicity of calculation radiating elements receive the plane wave coming from direction showed by angle Θ . This angle, during AF analysis, changes from 0° to 180° . There is no need to analyze the AF for angles from 180° to 360° because the result of that analysis would be a mirror reflection of the AF obtained for angles from 0° to 180° . When $\Theta = 90^\circ$ (for reference see Fig. 2.1) the radiating elements are located on the plane wave front. That means that signal received by every element has the same phase so the AF which is a sum of the received signals has its maximum for that angle (main beam direction). On the other hand, when the angle Θ has different value, array elements are located on different plane wave fronts. Therefore, the received signals have different phases and their sum is lesser then the sum obtained when received signals are in phase. That phase difference between received signals results from both angle, distance between the elements and the signal frequency.

2.1. Extended array factor model

In practice, the signals received by radiating elements are guided through different paths in order to achieve the desired radiation pattern. Each path introduces a phase shift and some amplification or attenuation to the received signal before signals are summed up at the output. By introducing constant progressive phase shift between the elements it is possible to achieve main beam direction different than 0° . On the other hand, the utilization of non-uniform amplitude distribution, e.g. chebyshev amplitude distribution, it is possible to lower the sidelobe level. Both effects are desired in the resulting AF. Phase shifts and changes in amplitude can be accumulated in N -element vectors $\bar{\psi}$ and \bar{a} , respectively. To model the amplitude change in the i -th path, the signal has to be multiplied by the i -th signal amplitude a_i . On

the other hand, the i -th phase shift ψ_i is introduced to the mathematical model as a multiplication by $\exp(j\psi_i)$. The extended mathematical model including the aforementioned multiplications is presented in equation 2.2 and its graphical explanation is shown in Fig. 2.2.

$$AF(\Theta, f, \bar{x}, \bar{a}, \bar{\psi}) = \sum_{i=1}^N a_i \exp\left(j\left(\frac{2\pi f}{c}x_i \cos \Theta + \psi_i\right)\right) \quad (2.2)$$

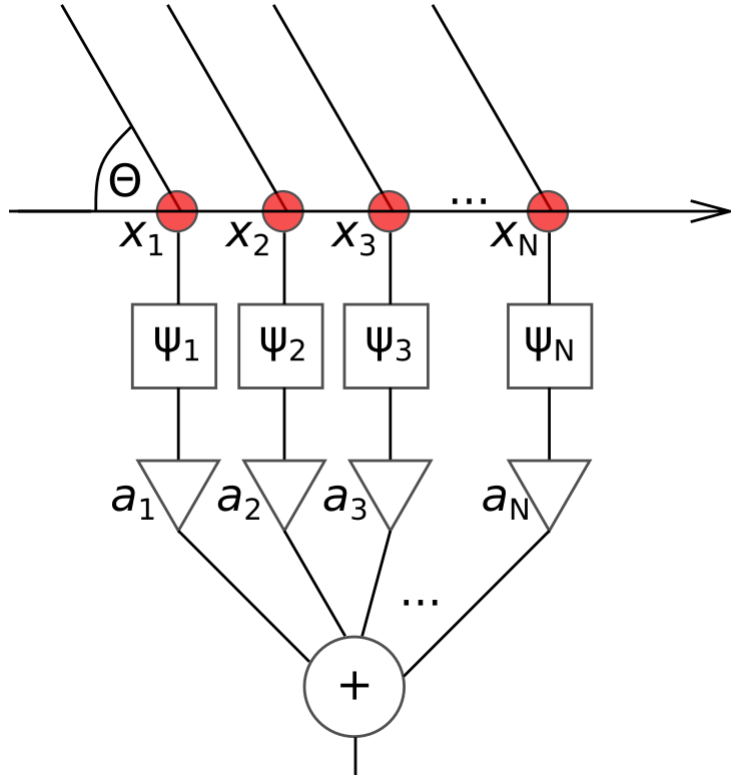


Fig. 2.2. Graphical explanation of extended AF model shown in equation 2.2.

At the outset it is worth to mention the convention of calculated AF visualization. For visualization purposes, the angle Θ is shifted by 90° . So the AF calculated for 0° is plotted for -90° . By applying this convention the plotted broadside beam points at 0° .

In order to visualize possible changes in AF, a four element array is considered. The distances between adjacent array elements are equal to $\lambda/2$ at the array's frequency of operation. Unmodified AF is obtained with the use of ideal radiating elements fed with signals having normalized amplitudes $\bar{a} = [1, 1, 1, 1]$ and phases $\bar{\psi} = [0^\circ, 0^\circ, 0^\circ, 0^\circ]$. Firstly, the amplitude is modified in such a way that inner elements are fed with signals having higher amplitude and outer elements are fed with signals having lower amplitudes. Exactly, the normalized amplitude vector $\bar{a} = [0.7, 1, 1, 0.7]$ was used to calculate the modified AF. Both unmodified and modified AFs are presented in Fig. 2.3 and as it is seen the sidelobe level is lower and the main beam is slightly wider when the tapered amplitude distribution is utilized. To show the progressive phase shift influence on the AF, phase vector $\bar{\psi} = [0^\circ, 45^\circ, 90^\circ, 135^\circ]$ was used and the obtained results are shown in Fig. 2.4. As observed, introducing progressive phase shift between array elements allows for changing the main beam direction.

In reality, antenna arrays are build with elements having either omnidirectional or directive radiation pattern. When the radiation pattern of the array's element and the AF are known, the theoretical radiation pattern of the antenna array can be calculated as their product. However, both the element radiation pattern and AF are usually expressed in dB. That means they are in logarithmic scale, so the computation is simpler because the multiplication is replaced by addition. In Fig. 2.5, the normalized AF, theoretical array radiation pattern and the array's element radiation pattern are shown. Since the element has a directive radiation pattern described by $\cos^{1.3}(\Theta)$, some AF parts (in this case sidelobes) are attenuated in the theoretical radiation pattern of the array.

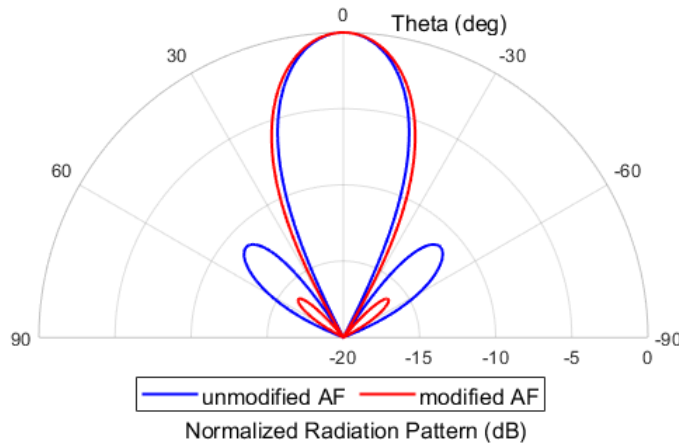


Fig. 2.3. Four element AFs with uniform and tapered amplitude distribution.

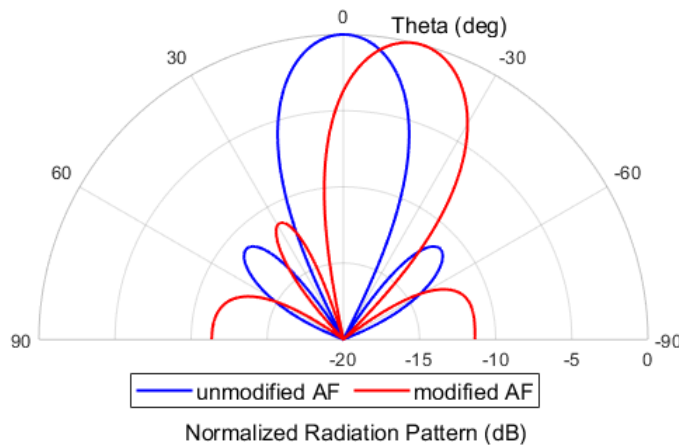


Fig. 2.4. Four element AFs with 0° and 45° phase progression.

2.2. Scalable antenna arrays theoretical analysis and the virtual radiating element model

For the scalable antenna arrays analysis, the extended AF model with a slight modification is used due to its simplicity and ability to solve more complex problems. As it was mentioned in Chapter 1,

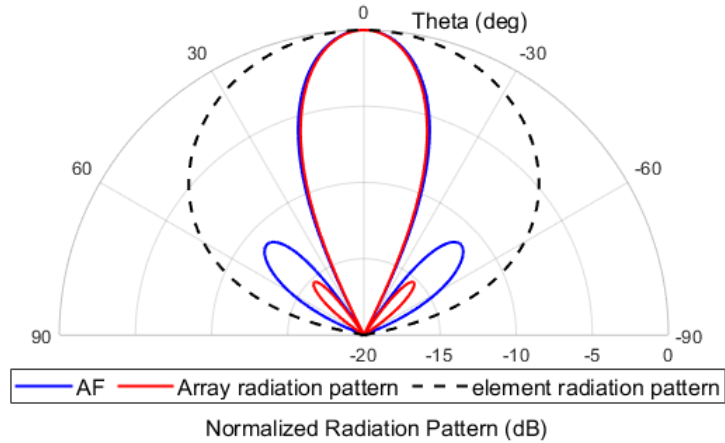


Fig. 2.5. Four element AF and the radiation pattern of an array composed of elements having directive radiation pattern.

scalable antenna arrays utilize signal switching in order to provide constant radiation characteristics such as beam direction and HPBW. Signal switching in AF calculation is implemented by changing the signal amplitudes \bar{a} throughout frequency range. In reality, passive circuits that realize the signal switching have some phase difference variation between the outputs but for calculation simplicity constant phase progressions or syn-phase signals are assumed.

Theoretical analysis can be realized in two different ways, namely the interpolating method and method utilizing the model of virtual radiating element. As a result of the theoretical analysis, the switching function is obtained. Both methods' initial steps are the same and include the frequency range choice and the radiating elements arrangement. In this work, only antenna arrays having octave band or multiple octave bands are discussed. In the case of multiple octave band antenna arrays the theoretical analysis is conducted on the lowest frequency octave and the resulting switching function is then scaled to higher frequency octaves. For one frequency octave radiating elements are placed in such a way that two subarrays can be distinguished one for the lower frequency f_L and one for the higher frequency $f_H = 2f_L$. These two subarrays are centered and the signal is switched in such way that at the lower frequency signal is fed to only first subarray and for the higher frequency the signal is fed only to the second subarray. Moreover, the subarrays are electrically similar which means that the relative distances between elements in the first subarray at the lower frequency are the same as the relative distances between elements in the second subarray at the higher frequency.

In the interpolating method, a number of frequencies are evenly selected from the frequency band. Chosen frequencies also include the lower and the higher frequencies. AFs for the boundary frequencies are the same if the signal is fully switched from first subarray at the lower frequency to the second subarray at the higher frequency. For chosen frequencies between the lower and the higher frequencies, the amplitudes are selected in such a way that the resulting AF has the beam direction and HPBW the same as the boundary AFs' beam direction and HPBW. If the parameters equality is unattainable, the amplitudes that allow for the best approximation of the boundary AFs' parameters should be selected.

During calculations, the amplitudes are normalized and the RF power is assumed constant in the entire frequency range because it allows for easier optimization. With such assumptions, equation 2.3 can be transformed into equation 2.4. Therefore, for determining the correct switching function, instead of two independent variables, one independent and one dependent variable are used.

$$a_{LF}^2(f) + a_{HF}^2(f) = 1 \quad (2.3)$$

$$a_{HF}(f) = \sqrt{1 - a_{LF}^2(f)} \quad (2.4)$$

where

a_{LF}^2 – normalized amplitude of signals driving elements in the first subarray,

a_{HF}^2 – normalized amplitude of signals driving elements in the second subarray,

f – the signal frequency.

After the amplitudes for selected frequencies are found, their values are used to interpolate the switching function over the entire frequency band. To interpolate the switching function, polynomials are used. For interpolation process, frequencies are normalized which means that normalized frequencies are in range from 1 to 2. Frequency normalization is used, in order to allow simple switching function scaling to other frequency octaves.

In order to understand the second method for obtaining switching function, the virtual radiating element model has to be presented and explained. In scalable antenna arrays, groups of fixed radiating elements between which the RF signal is switched can be distinguished. Each of these groups can be seen as one virtual radiating element that changes its position throughout frequency range. The position of the virtual radiating element is expressed in equation 2.5.

$$x_v(f) = \frac{\sum_{i=1}^N a_i^2(f)x_i}{\sum_{i=1}^N a_i^2(f)} \quad (2.5)$$

where

$x_v(f)$ – virtual radiating element position,

N – number of radiating elements in group,

$a_i(f)^2$ – amplitude at the input port of i-th fixed radiating element,

x_i – i-th radiating element position.

For visualization purposes an 8 element octave-band scalable antenna array shown in Fig. 2.6 is considered. This array consists of two subarrays one operating at the lower frequency f_L (array composed of blue elements) and one operating at the higher frequency f_H (array composed of red elements and

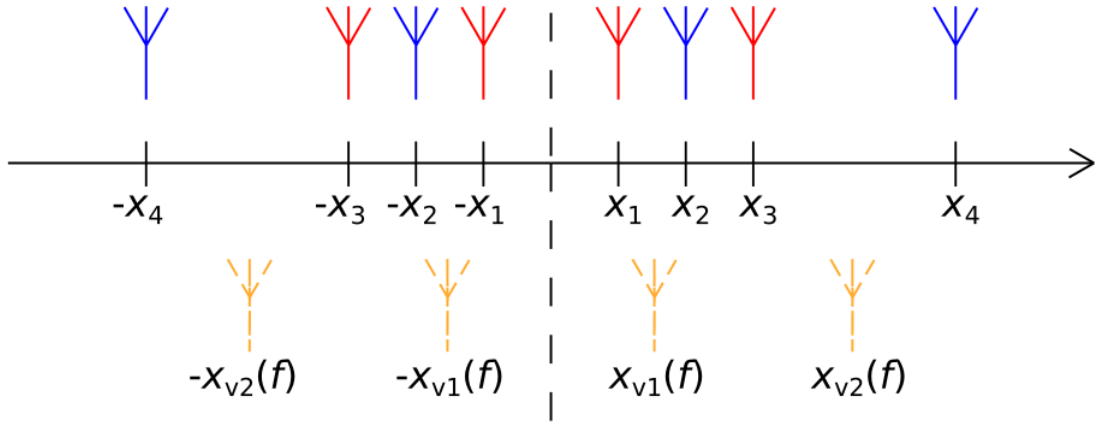


Fig. 2.6. 8 element octave-band scalable antenna array and its approximation with a 4 element array composed of virtual radiating elements.

$f_H = 2f_L$). The subarrays are centered and relations between array elements' positions are shown in equations system 2.6.

$$\begin{cases} x_2 = 2x_1 \\ x_3 = 3x_1 \\ x_4 = 3x_2 \\ x_1 = \lambda/4 \text{ at } f_H \end{cases} \quad (2.6)$$

From the system of equations 2.6, it follows that distances between adjacent red elements are equal to $\lambda/2$ at f_H whereas distances between adjacent blue elements are equal to $\lambda/2$ at f_L . Moreover, in the antenna array 4 pairs of elements, with following positions: $\{-x_4, -x_3\}$, $\{-x_2, -x_1\}$, $\{x_2, x_1\}$ and $\{x_4, x_3\}$, can be distinguished. The RF signal is switched between elements in each pair, so each pair can be viewed as one radiating element according to the virtual radiating element model. Positions of virtual elements are: $-x_{v2}(f)$, $-x_{v1}(f)$, $x_{v1}(f)$ and $x_{v2}(f)$.

The switching function can be selected in such a way that for the entire frequency range $x_{v2}(f)$ is equal to $3x_{v1}(f)$ which means that the virtual array is seen as electrically similar array for every frequency in the octave band. For this purpose, only one pair of elements has to be analyzed because for every other pair the result is the same. The way for determining the switching function is described with use of elements placed in positions x_1 and x_2 . These two elements have known positions and are seen as one placed in $x_{v1}(f)$. This virtual radiating element position is described in equation 2.7.

$$x_{v1}(f) = \frac{a_1^2(f)x_1 + a_2^2(f)x_2}{a_1^2(f) + a_2^2(f)} \quad (2.7)$$

Furthermore, for each frequency in the frequency octave $x_{v1}(f)$ is equal to $\lambda/4$ for that frequency, so it is a known variable. Similarly in this case, dependencies from equations 2.3 and 2.4 can be used. By applying these dependencies, the switching function can be derived as it is shown in equation 2.8.

$$a_1(f) = \sqrt{\frac{x_{v1}(f) - x_2}{x_1 - x_2}} \quad (2.8)$$

The switching function obtained with the use of the model of virtual radiating element, that is presented with resultig AFs in Fig. 2.7 , is derived for every frequency in the entire bandwidth. Therefore, the method utilizing the model of virtual radiating element allows for more precise determination of the switching funciton. The resulting AFs feature HPBW variation not greater than $\pm 2.8^\circ$ and side lobe level equal to -10 dB in the worst case. However, the attained switching function can be optimized and therefore, the side lobe level and HPBW variation can be reduced.

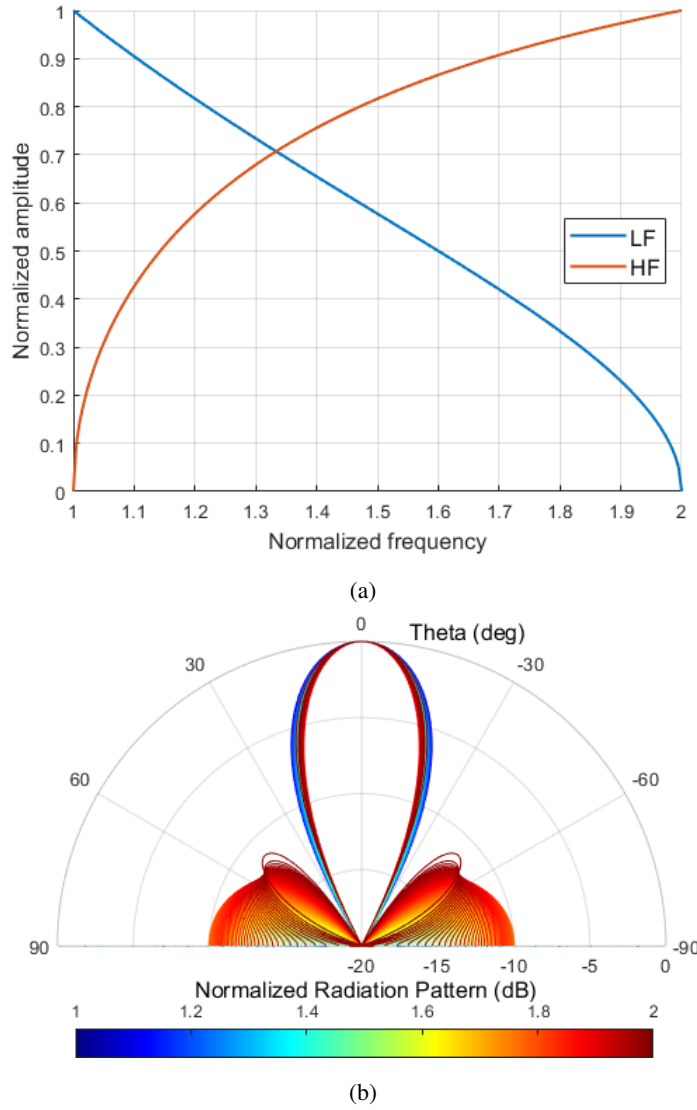


Fig. 2.7. The switching function obtained with the method utilizing the model of virtual radiating element (a) and the AFs calculated with use of the presented switching function (b).

In Fig. 2.8 the optimized switching function and the resulting AFs are presented. As it is seen, the switching function after optimization has a slightly different shape. The change in the shape is important, since the optimized switching function is easier to implement in the real passive microwave circuits.

Moreover, the resulting AFs are better since the HPBW variation and the sidelobe level in the worst case are reduced to $\pm 0.3^\circ$ and -11.5 dB, respectively.

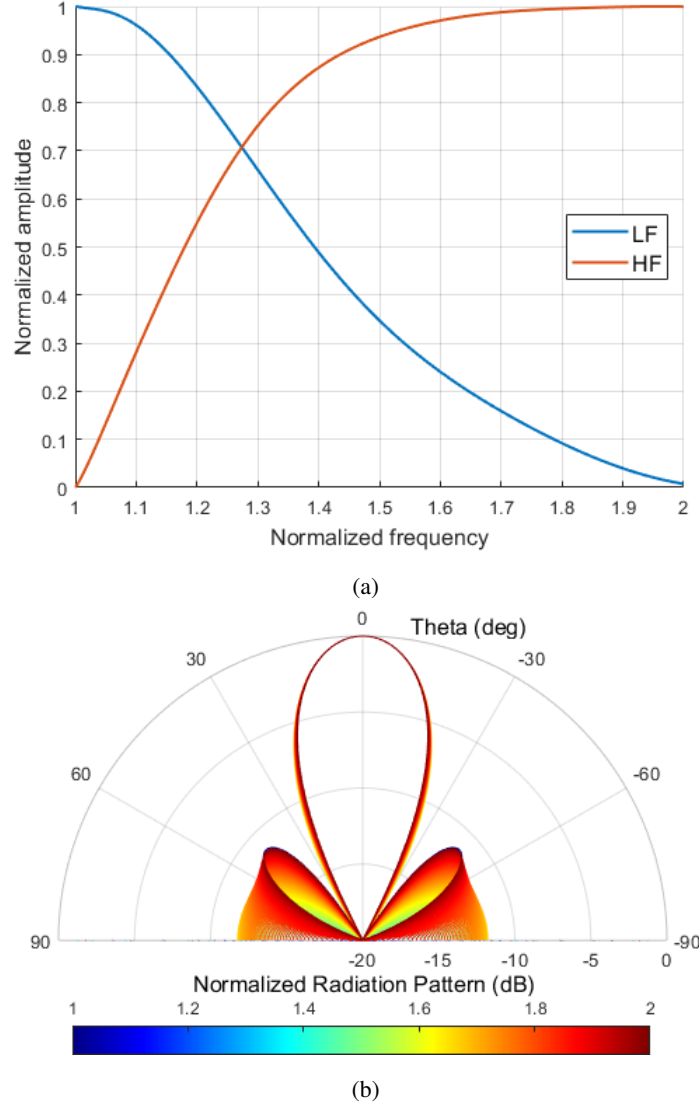


Fig. 2.8. The optimized switching function obtained with the method utilizing the model of virtual radiating element (a) and the AFs calculated with use of the presented switching function (b)

The attained AFs are similar. In cases of both optimized and unoptimized switching functions, AFs values for angles around -90° and 90° are rising with the frequency increase. This effect may seem to have a negative impact on the real array radiation pattern. However, the effect of the narrower element's radiation pattern for higher frequencies counteracts the observed effect in the AF. Moreover, beam direction variation was not observed in both analyzed AFs since in theoretical analysis, beam direction variation is observed only for tilted beams.

The interpolating method can yield similar results to the results obtained with use of the method utilizing the model of virtual radiating element. However, it has to be underlined that results obtained with the interpolating method are less accurate. Although, the method utilizing model of virtual radiating element is better for the analysis of scalable antenna arrays, the interpolating method was used for analysis of the arrays in Chapter 3. It results from the fact that the antenna arrays discussed in Chapter 3 were analyzed and designed before the model of virtual radiating element was developed. However, the method utilizing the model of virtual radiating element was used for analysis of the antenna array discussed in Chapter 4.

3. Multibeam scalable antenna arrays

In this Chapter, the designed multibeam scalable antenna arrays are discussed. All the designed scalable antenna arrays operate in frequency range from 2 GHz to 4 GHz and utilize the same radiating elements, namely the linearly tapered slot antennas (LTSA). The design process and parameters of LTSA are thoroughly discussed in Section 3.1. The antenna elements are properly spaced and fed by feeding networks composed, i.e., of Butler matrices and directional filters. Depending on the scalable antenna array concept, different Butler matrices are used, however, in every proposed feeding network the same directional filters, which are reviewed in Section 3.2, are utilized. In Section 3.4, two four-beam scalable antenna arrays are presented. The description of each antenna array begins with the presentation of the concept in which arrangement of radiating elements and feeding networks are shown. Moreover, the results of theoretical analysis and measurements of the developed antenna arrays are discussed. Similarly, three three-beam scalable antenna arrays are presented in Section 3.5.

3.1. Radiating element

The presented concepts of scalable antenna arrays require the application of radiating elements, which could be arranged in the distance equal to 0.25λ at a higher frequency of operational bandwidth (in most considered arrangements $f_h = 4$ GHz). Moreover, each radiating element should feature a good impedance match in the entire bandwidth. In cases of multi-beam antenna arrays as well as first and $N + 1$ subarrays in multi-octave broadside beam scalable antenna array presented in Chapter 4 required operating bandwidth for each radiating element equal to an octave of frequency. In comparison, radiating elements operating in intermediate subarrays in the concept presented in Figure 4.3 should feature return loss better than 10 dB in bandwidth greater than one octave. Furthermore, a wideband impedance match is insufficient for multi-beam antenna arrays which necessitate broad beamwidth in the operating frequency range allowing improvement of sidelobe level, especially for $L & R$ beams of the twelve-element array where phase progression is equal to 135° . Besides, HPBW of radiating elements should not change significantly in the required bandwidth in order to obtain a stable radiation pattern over the entire bandwidth.

The Linearly Tapered Slot Antenna (LTSA) had been chosen to meet the requirements. The radiating element has been developed based on similar LTSA presented in [19]. The antenna is excited through a gradually tapering microstrip line and slot line, which create a transition structure resembling

an impedance transformer. The feed line consists of three sections of transmission line each one has a different characteristic impedance arranged in such a way the first section has 50Ω , the second has 61Ω , and the third one has 94Ω , while the slot line characteristic impedance is equal to 110Ω , physical dimensions are shown in Tab 3.1. Furthermore, electrical length of the second and third sections of the feed line is around 90° at the first resonant frequency f_{r1} . Moreover, the total length of feed line is around $\frac{\lambda}{2}$ and $\frac{3\lambda}{4}$ at the first f_{r1} and second resonant frequencies f_{r2} , respectively. The transmission line is arranged in such a way that the middle of the narrowest section is above the slot line, and the stub length is equal to $\frac{\lambda}{8}$ at f_{r1} . Length of the slot line and vertical position of the feed line have been determined in optimization process in such a way to create an area under slot line and widths equal to the slot line width, where is a region with minimum magnitude of E filed in the entire operating frequency range on the plane containing radiating structure.

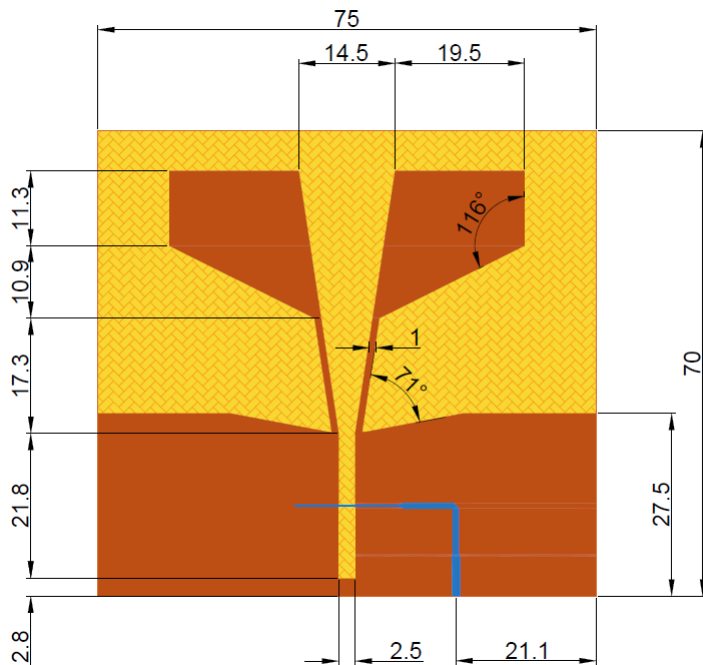


Fig. 3.1. Layout of the designed LTSA radiation element. The dimensions are given in mm.

TABLE 3.1. Physical dimensions of the feedline in the developed radiation element, where L is length and W is width of the line.

Dimension	Value (mm)
L_1	5.8
W_2	1.195
L_2	15.6
W_2	0.8
L_3	16
W_3	0.3

TABLE 3.2. Simulated parameters of the radiating element shown in Fig. 3.1

	2 GHZ	2.5 GHZ	3 GHz	3.5 GHZ	4 GHZ
Radiation Efficiency	90.7%	91.8%	90.3%	88.9%	86.6%
Front to Back Ratio	4.3 dB	8.9 dB	13.4 dB	6.9 dB	7.3 dB
Peak Gain	2.3 dBi	2.8 dBi	3.1 dBi	3.6 dBi	3.8 dBi
Peak Directivity	2.7 dB	3 dB	3.5 dB	4 dB	4.6 dB
H-Plane HPBW	205°	183°	161°	138°	109°
E-Plane HPBW	84°	89°	93°	87°	67°

The radiating part of the developed structure consists of two separate wings and transmission lines, which lead coupled signal. The analysis of the designed radiating structure allows for making a few observations. Firstly, the distance between wings significantly affects the HPBW and the directivity of radiating elements. Moreover, the wings area has influenced the basic parameters of an antenna, such as radiated efficiency, front to back ratio, directivity, HPBW and gain. The simulated parameters of the developed radiating element are shown in Table 3.2 for five discrete frequency points in the required bandwidth. The designed radiating element was manufactured and measured. FR4 dielectric laminate, having the dielectric constant 4.4 with a thickness of 0.508 mm was used. As it is seen in Fig 3.3 and Fig 3.2 designed radiation element features good impedance match in the required bandwidth and wide half power beamwidth with a stable radiation pattern across the entire bandwidth.

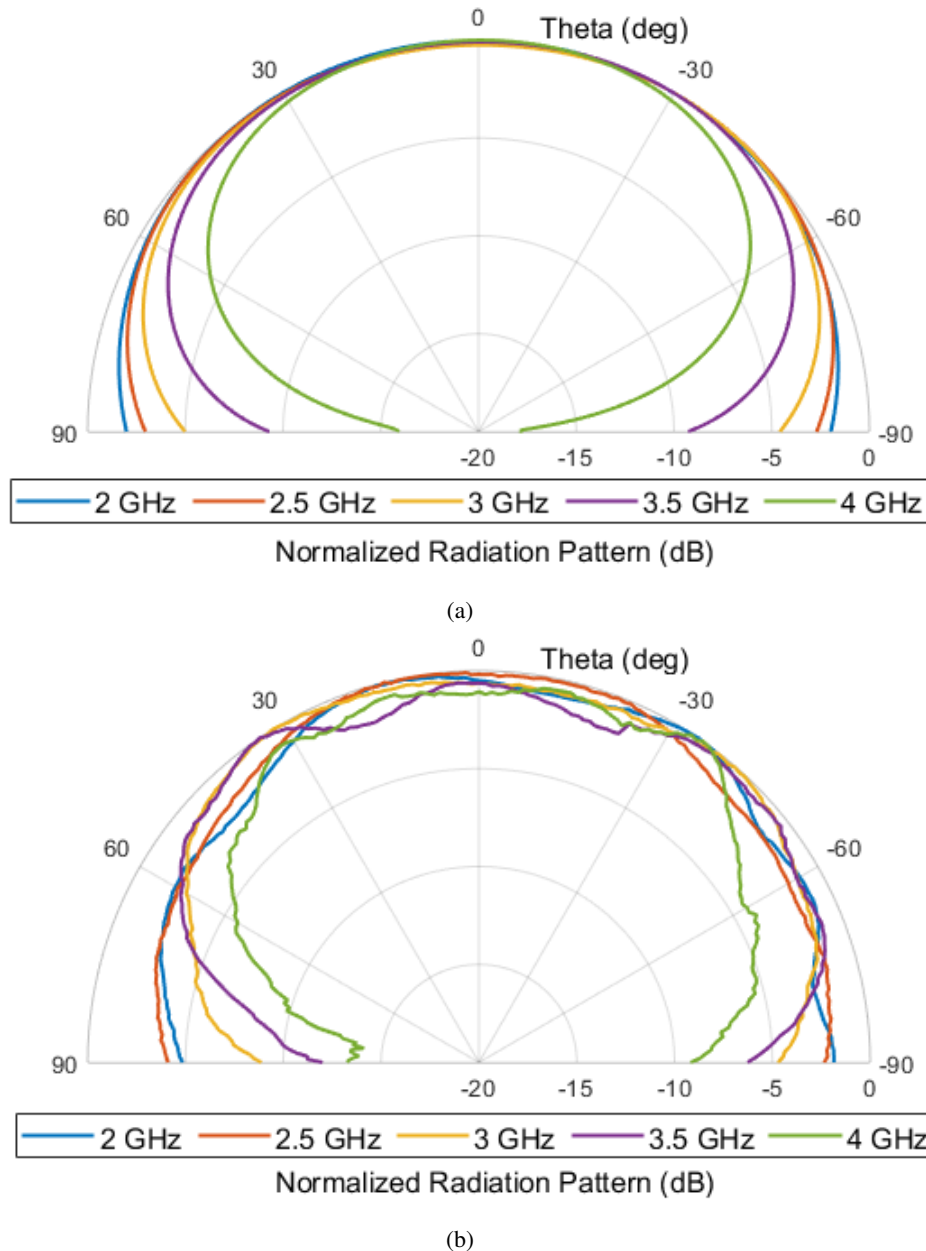


Fig. 3.2. Simulated (a) and measured (b) radiation patterns of the developed LTSA.

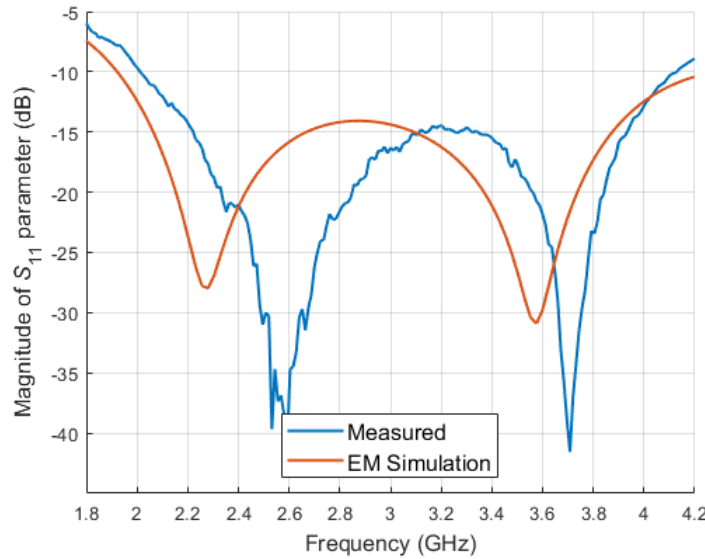


Fig. 3.3. Simulated and measured reflection coefficient of the developed LTSA.

3.2. Directional filter

Design process of the directional filter utilized in the feeding network of the scalable antenna array begins with the determination of the switching function. In case of this particular directional filter the switching function, that is presented in Fig. 3.4, was obtained with the use of the interpolating method. The switching function between 1 and 2 (normalized frequency octave) is interpolated by a polynomial 3.1:

$$LF(\underline{f}) = -0.3\underline{f}^3 + 1.95\underline{f}^2 - 4.75\underline{f} + 4.12 \quad (3.1)$$

where

$LF(\underline{f})$ – normalized amplitude feeding the elements operating in the lower subband of operational frequency range,

\underline{f} – normalized frequency.

After the switching function is attained, the microwave circuit that can reproduce the function has to be designed. In this case, the developed directional filter is based on the design presented in [9]. The schematic diagram of the discussed filter is presented in Fig. 3.5,

The directional filter consist of two coupled line sections, each having different coupling coefficient, and two quarter-wave transmission lines in between. These four elements switch the signal gradually from one output to the other one in one frequency octave, however the phase difference between the outputs is not acceptable. In order to achieve in-phase signals at the directional filter outputs, the phase shifters are connected to each output. To one output the Schiffman C-section is connected, whereas, to

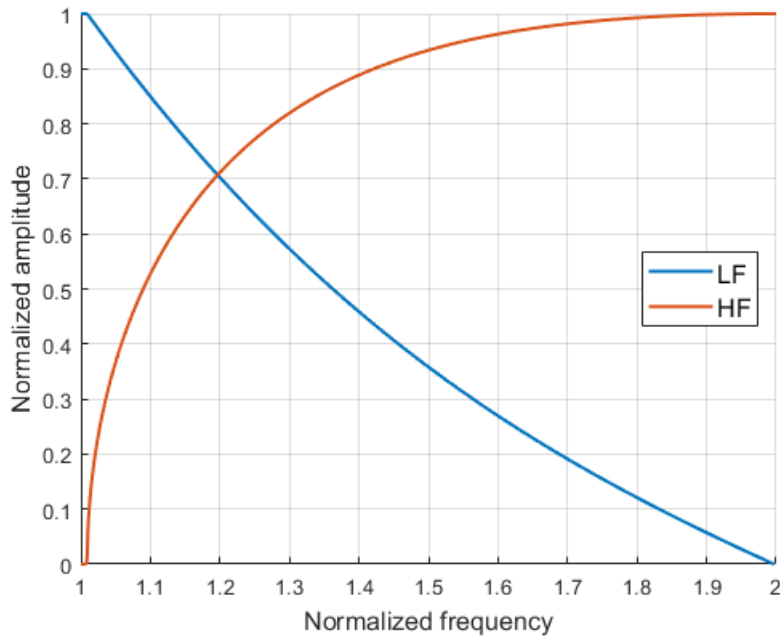


Fig. 3.4. Switching function obtained with use of the interpolation method.

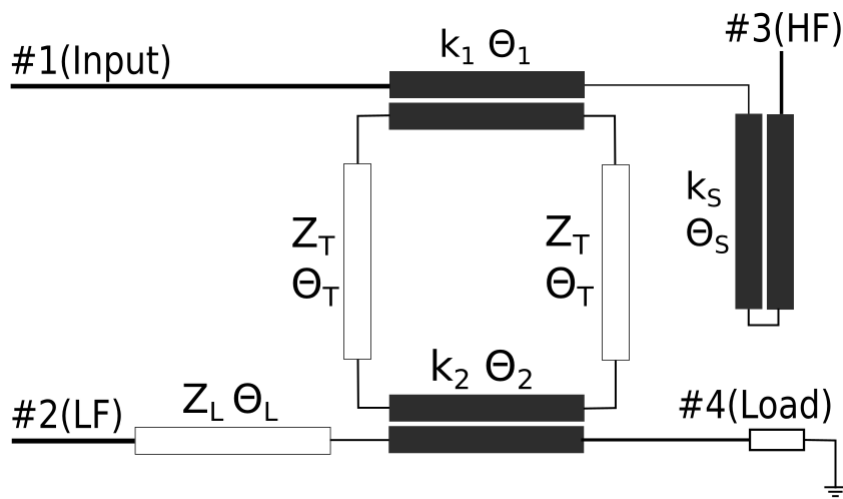


Fig. 3.5. Schematic diagram of the developed directional filter.

the other one a transmission line is attached. The element parameters marked in Fig. 3.5 are shown in Table 3.3. The proposed directional filter is universal for every octave frequency range. In order to utilize the proposed directional filter in a specific octave range, the dielectric structure in which the filter will be manufactured has to be chosen. Then, the physical dimensions of elements can be calculated from parameters, such as the dielectric constant and thickness of dielectric laminate.

For the development of the directional filter, a stripline structure was chosen. The selection results from the requirements for high coupling between the coupled lines in the directional filter. Such high coupling cannot be realized by edge coupled lines, therefore a microstrip structure cannot be chosen.

TABLE 3.3. Electrical parameters of elements constituting the directional filter.

Parameter	Value ^a
k_1	0.818
k_2	0.793
k_S	0.784
Z_T	50Ω
Z_L	50Ω
Θ_1	90.0°
Θ_2	90.0°
Θ_S	59.8°
Θ_L	298.0°
Θ_T	90.0°

^a The electrical lengths are given for the lowest frequency in the octave band.

However, in a stripline structure, coupled lines can be placed on two sides of a thin dielectric laminate which allows for increasing the resulting coupling. Therefore, the stripline structure is suitable for the development of such a filter.

The directional filter was developed in a homogeneous symmetric stripline structure. The structure consists of three dielectric laminate layers arranged in such a way that a thin laminate with a thickness $h_2 = 0.1$ mm is inserted between two thick layers with a thickness $h_1 = 1.52$ mm. All layers have the same dielectric constant equal to 3.38. The layout of the developed directional filter and the schematic cross-sectional view of the utilized dielectric structure are shown in Fig. 3.6.

The designed directional filter was manufactured and measured. The obtained measurement results in comparison to the ones obtained in electromagnetic simulations are shown in Fig. 3.7. As it is seen, the measurement results are in line with the simulation results and the appropriate switching function is achieved. Moreover, the developed directional filter features good impedance match in the entire bandwidth and the resulting differential phase imbalance is not greater than $\pm 10^\circ$. It has to be underlined that although greater differential phase imbalance is observed around 2 GHz and 4 GHz frequencies, this phase imbalance has a negligible impact, since the amplitude difference between the outputs is large. In summary, the developed directional filter faithfully reproduces the switching function from Fig. 3.4 and features low phase imbalance. Moreover, such a filter is relatively easy to design and manufacture. Therefore, it can be utilized as a part of feeding networks of the one-octave scalable antenna arrays.

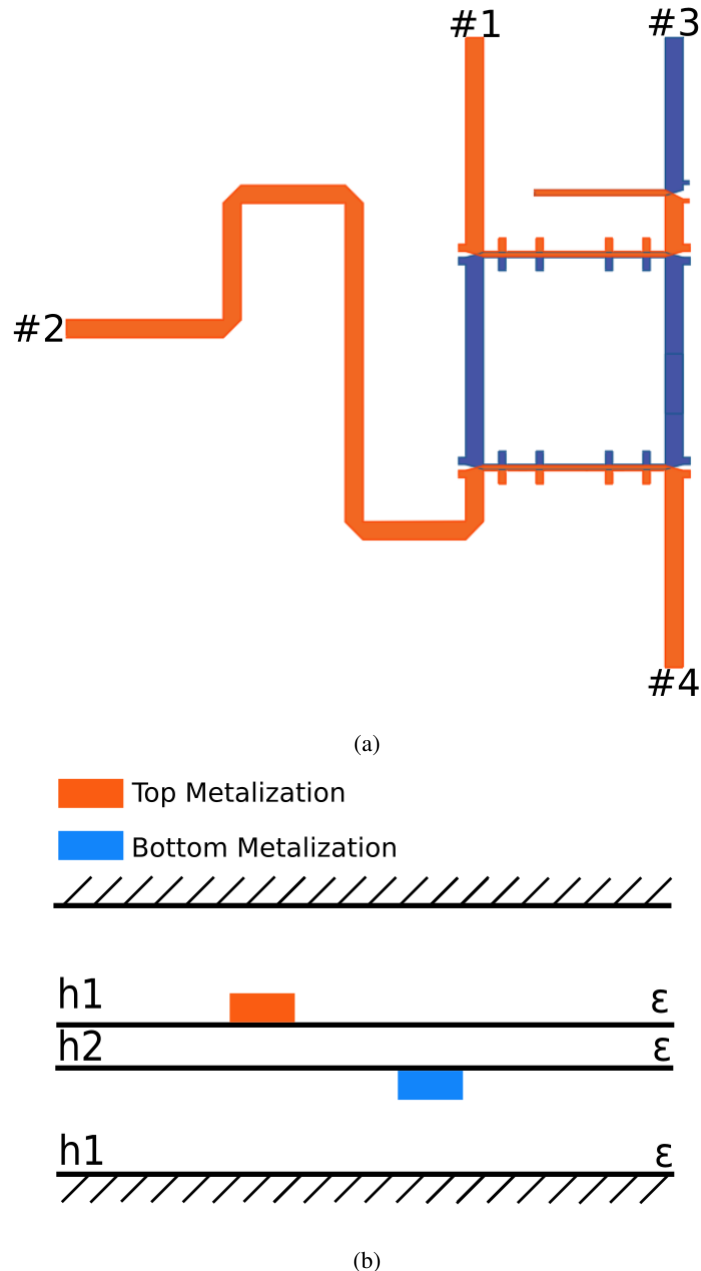


Fig. 3.6. The layout of the developed directional filter (a) and the schematic cross-sectional view of the utilized stripline dielectric structure.

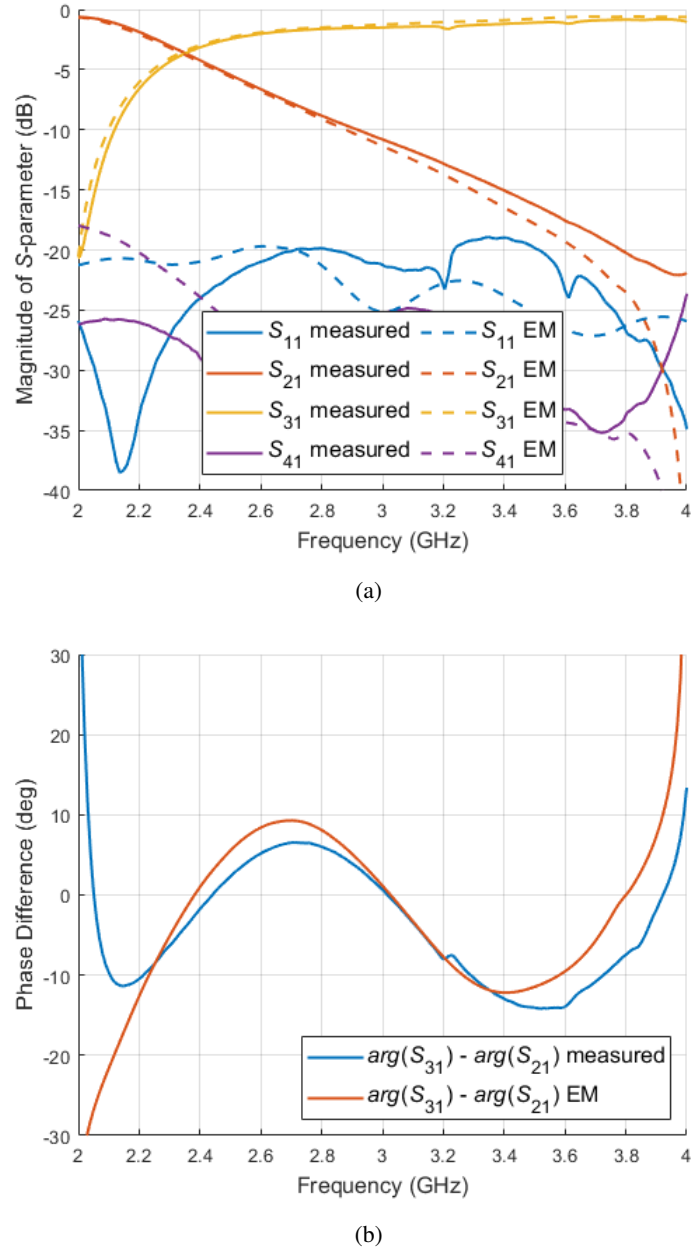


Fig. 3.7. Measured and simulated magnitude (a) and differential phase (b) characteristics of the developed directional filter.

3.3. T-junction power divider

The T-junction power divider is used in the concept of simultaneously power division, which allows the extension of the amount of radiating elements from 8 to 12 and achieves theoretically a lossless feeding network for the antenna array. The additional power division is realized in the octave band (2–4 GHz), and power division is unequal to ensure appropriate signal distribution. Theoretical analysis of the 12-element multibeam antenna system has led to the conclusion that the power division should be realized in the ratio of 5.6:1, which means that the signal at the second port is approximately 0.7 dB lower and at the third port 8.2 dB lower than at the first port (input). A source impedance of 50Ω has been chosen for lossless T-junction power divider. Assuming voltage at the junction point like a V_0 , knowing the source impedance Z_0 and the ratio of power division, characteristic impedance of transmission lines were determined base on the following equations:

$$P_{in} = \frac{1}{2} \frac{V_0^2}{Z_0}$$

$$P_2 = \frac{1}{2} \frac{V_0^2}{Z_2} = 0.73 P_{in}$$

$$P_3 = \frac{1}{2} \frac{V_0^2}{Z_3} = 0.27 P_{in}$$

$$Z_2 = \frac{100}{27} Z_0 = \frac{20}{3} Z_0 = 185 \Omega$$

$$Z_3 = \frac{100}{73} Z_0 = \frac{20}{17} Z_0 = 68 \Omega$$

Based on the determined characteristic impedances, it could be concluded that the lines with an impedance equal to 185Ω are not feasible. Therefore, it has been decided to make a divider assuming the source impedance equal to 50Ω , but dividing the power on the divider where Z_0 equals 25Ω . Thus, the characteristic impedances of the transmission lines in the redesigned divider are respectively:

$$Z_0 = 25 \Omega$$

$$Z_2 = 34 \Omega$$

$$Z_3 = 92 \Omega$$

Implementation of the designed power divider requires matching network to the system, which is 50Ω . for this purpose, two section impedance transformers have been connected to the 50Ω transmission line in order to obtain good impedance match throughout the operating bandwidth. All electrical lengths of the transmission line are equal to 90° at the center frequency 3 GHz. A power divider with an additional phase shifter to compensate for the delay have been designed on Arlon 25N substrate with the dielectric constant of 3.38 and thickness of 1.524 mm. The dimensions of the designed and fabricated microstrip quarter-wave transformers are given in Table 3.2.

TABLE 3.4. Physical and electrical parameters of a T-junction power divider and two-section quarter-wave transformers.

	W_1	W_2	W_3	W_4
$50 \Omega \Rightarrow 25 \Omega$	3.51 mm	4.67 mm	7.22 mm	9.31 mm
	50 Ω	41 Ω	30 Ω	25 Ω
	W_5	W_6	W_7	W_1
$34 \Omega \Rightarrow 50 \Omega$	6.17 mm	5.4 mm	4.16 mm	3.51 mm
	34 Ω	37 Ω	44 Ω	50 Ω
	W_8	W_9	W_{10}	W_1
$90 \Omega \Rightarrow 50 \Omega$	1.14 mm	1.62 mm	2.67 mm	3.51 mm
	92 Ω	77 Ω	59 Ω	50 Ω

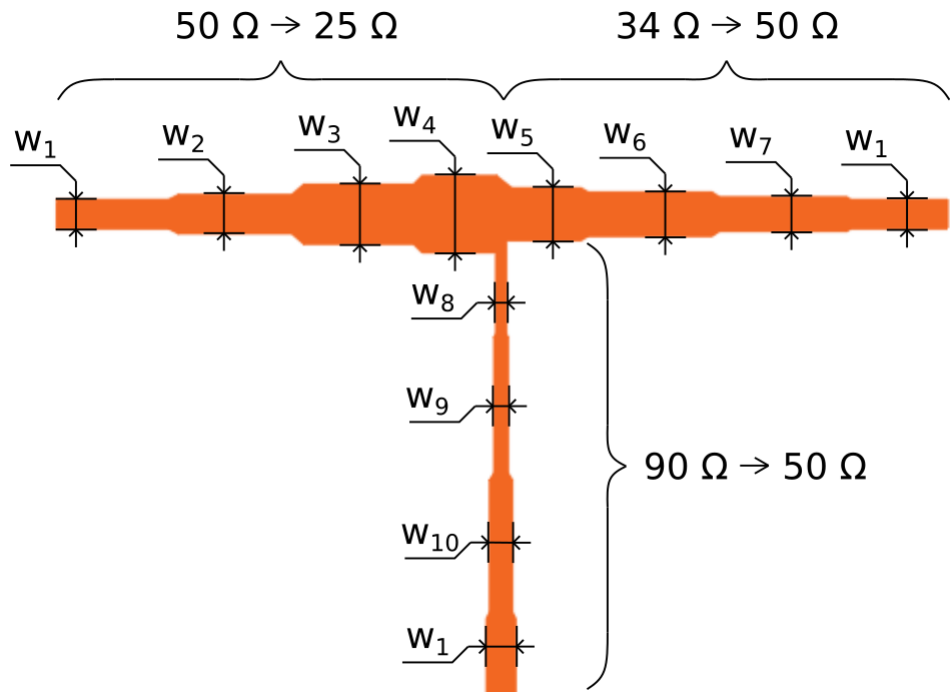


Fig. 3.8. Layout of a T-junction power divider.

The frequency characteristics of the designed and manufactured divider are shown in Fig 3.9. The result obtained in the measurements are similar to the results of EM simulation. The designed power divider implements the appropriate power distribution and is characterized by a good impedance match in the required operating band.

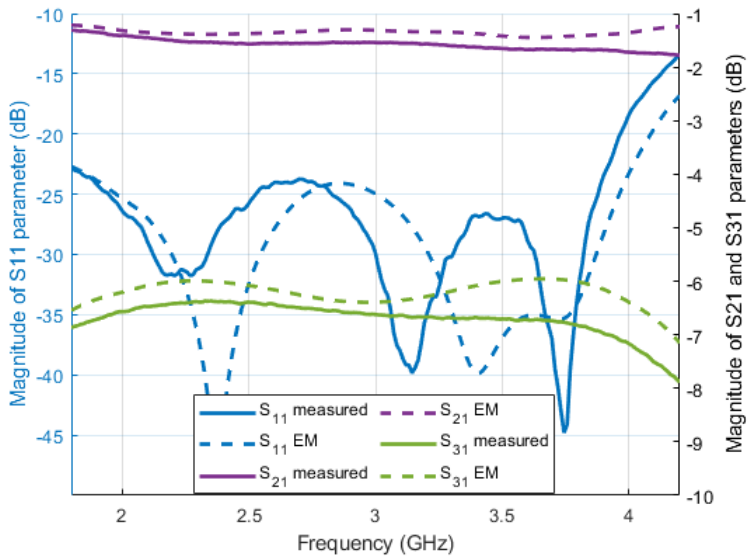


Fig. 3.9. Measured and simulated magnitude characteristics of the developed T-junction power divider.

3.4. Four-beam antennas

In this Section, two developed concepts of four-beam scalable antenna arrays are presented starting from the eight-element antenna array fed by a lossy network. Moreover, in order to develop a theoretically lossless feeding network, the concept of eight-element antenna array was extended to the concept of twelve-element antenna array. These concepts were the subject of the published paper [15] where they are thoroughly explained.

3.4.1. 8-element array

The concept of the four-beam eight-element scalable antenna array is presented in Fig. 3.10. The antenna array consists of two distinct centered four-element subarrays one for the lower frequency ($f_l = f_0$) composed of blue radiating elements and one for the higher frequency ($f_h = 2f_0$) composed of red elements. The subarrays are electrically similar at boundary frequencies which means that the distances between blue radiating elements and red ones relative to wavelength at the lower and higher frequency, respectively, are equal. The distances between the red elements d are equal to 0.45λ at $2f_0$, whereas distances between blue elements are equal to $2d$ ($2d = 0.9\lambda@2f_0 = 0.45\lambda@f_0$). Therefore, the scalable antenna array can operate in a 2:1 BW. The scalable antenna array is fed by a feeding network composed of a broadband 4×4 Butler matrix to which outputs directional filters are connected. Such a feeding network allows for achieving four independent beams, since the Butler Matrix ensures constant phase shifts between outputs ($\pm 45^\circ$ and $\pm 135^\circ$) and the resulting phase shift depends on which input port the signal is applied. Whereas the directional filters gradually switch the signal between elements that should be driven by the in-phase signal. As it is seen in Fig. 3.10, the feeding network can be extended by two

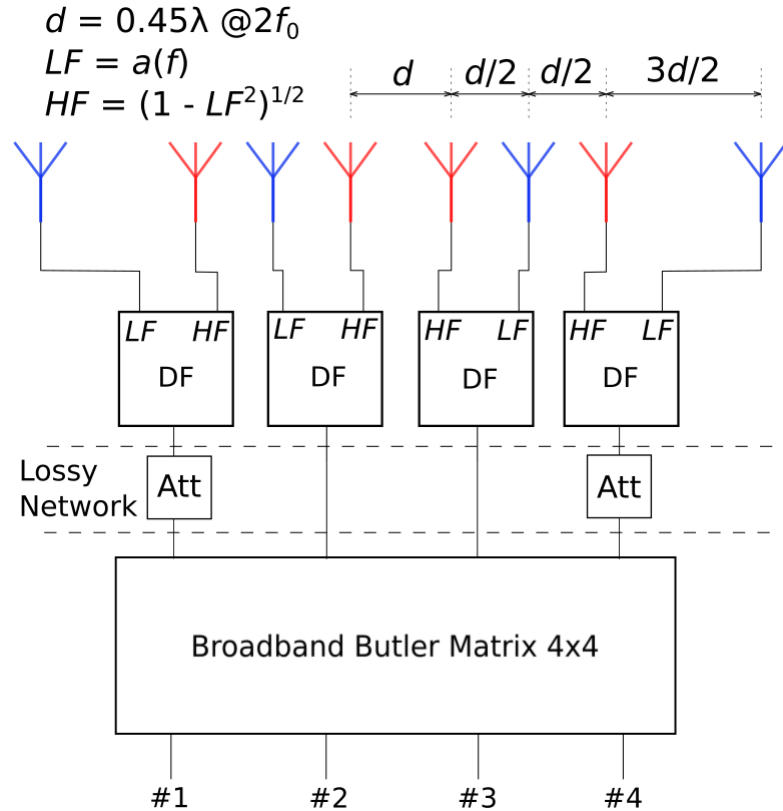


Fig. 3.10. Concept of an eight-element four-beam scalable antenna array.

attenuators. These attenuators are placed in path of the signal driving the outer scalable antenna array's elements and the resulting radiation pattern can be improved by proper selection of their values.

The scalable antenna radiation pattern were analyzed assuming an ideal feeding network, that utilizes directional filters realizing the switching function shown in Fig. 3.4, and the simulated radiation patterns of the radiating element described in Section 3.1. Firstly, the attenuators were omitted and the resulting normalized radiation patterns are presented in Fig. 3.11. As it is seen, all beams, i.e., 1L&1R and 2L&2R are stable in the octave frequency range. However, the resulting sidelobe level is relatively high, and in the calculations negative effects such as the coupling between the adjacent radiating elements, that can worsen the resulting radiation pattern, were not included. It is worth underlining that the highest sidelobe is observed for 0° . It results from the AF itself, since for such radiating element's placement the sidelobe for 0° is present. However, the use of directive radiating element has a negative effect on the sidelobe level, since the radiating element's radiation pattern has its maximum at exactly 0° . Therefore, the utilized radiating element has to feature stable radiation pattern across the operational frequency range. In this case, the most important parameter of the radiation pattern is the HPBW because the wider the HPBW is, the lower will be the attenuation of the main beam and the resulting sidelobe level will be better.

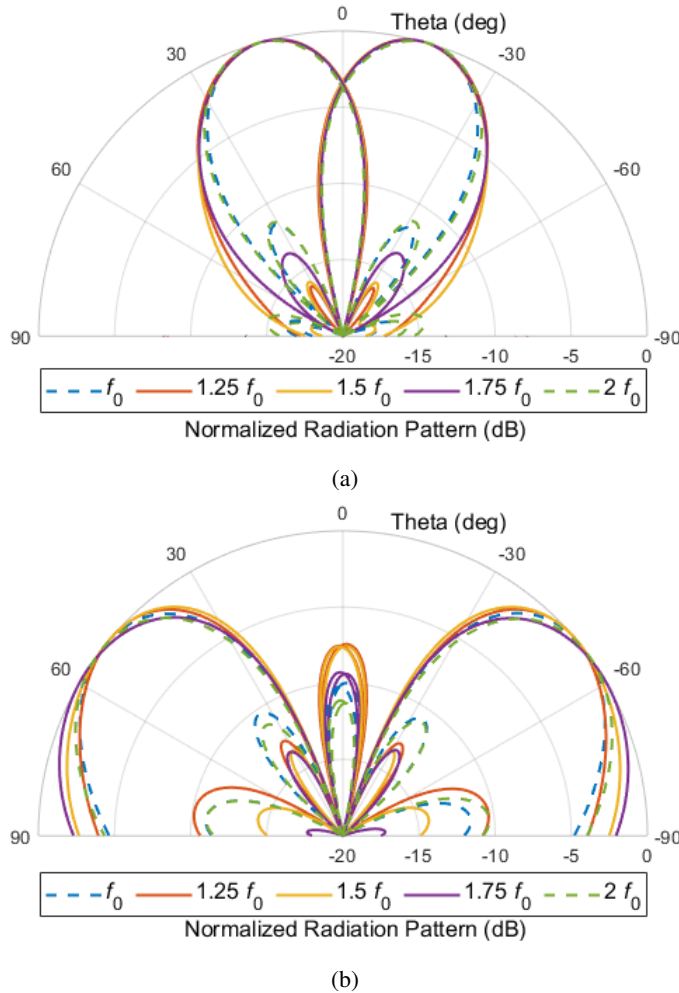


Fig. 3.11. Calculated 1L&1R beam (a) and 2L&2R beam (b) radiation patterns for a scalable antenna array depicted in Fig. 3.10 without a lossy network. For calculations the simulated radiation pattern of the antenna element described in Section 3.1 was assumed.

To lower the sidelobe level observed in the radiation pattern, the nonuniform amplitude distribution across the array's elements was utilized, by adding the attenuators in the outer signal paths. The attenuation level was analyzed and 3-dB attenuators were chosen to extend the feeding network, as presented in Fig. 3.10. It is worth underlining that by adding two 3-dB attenuators in outer signal paths the whole signal is attenuated by only 1.25 dB. The radiation patterns were calculated and are shown in Fig. 3.12. As predicted the resulting sidelobe level is significantly lower. However, as it was described in Chapter 2, the utilization of unequal power distribution across the radiating elements not only reduces the sidelobe level, but also widens the main beam. As a result the observed grating lobes (only for 2L&2R beams) also get wider and higher, but their values are acceptable since they are better than -8 dB. The obtained radiation patterns are stable across one-octave frequency range.

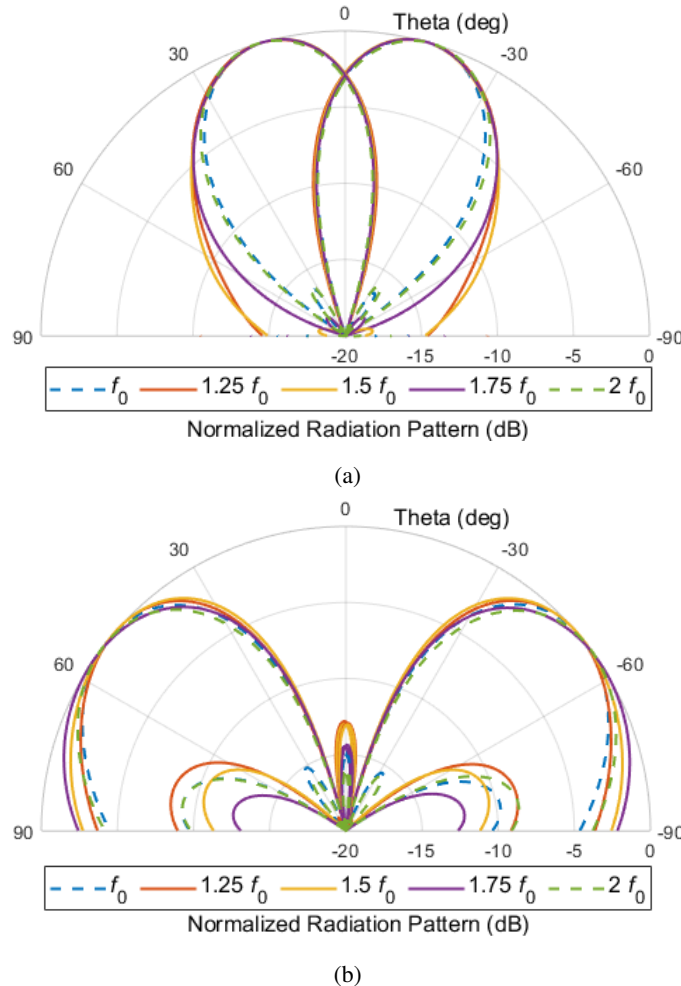


Fig. 3.12. Calculated 1L&1R beam (a) and 2L&2R beam (b) radiation patterns for a scalable antenna array depicted in Fig. 3.10 with a lossy network. For calculations the simulated radiation pattern of the antenna element described in Section 3.1 was assumed.

To verify the theoretical analysis the scalable antenna array operating in 2 – 4 GHz frequency range with the proper feeding network were assembled. The feeding network was composed of a 4×4 broadband Butler matrix that was presented in [20] and directional filters discussed in Section 3.2. The Butler matrix features both isolation and return loss better than -20 dB and its transmission imbalance in the frequency rage of interest does not exceed ± 1 dB/ 8° . The assembled scalable antenna array was mounted in a 3D-printed rail on the front side of the robotic arm in an anechoic chamber, whereas the feeding network was placed on the back of the robotic arm as depicted in Fig. 3.13. To avoid negative effects that could have been introduced by metal elements, plastic screws were used to mount the radiating elements in the rail. The antenna array's radiation patterns were measured with the use of 2 port vector network analyzer (VNA). First port of the VNA was connected to the reference horn antenna, whereas the second port was connected to one of the Butler matrix ports. Since the Butler matrix has four input/output ports to properly measure the radiation patterns it was necessary to conduct four distinct measurements one

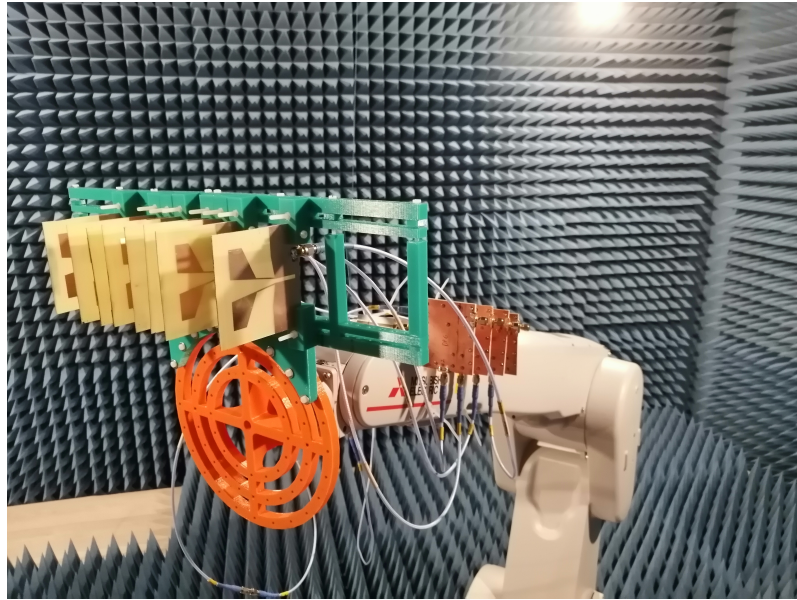


Fig. 3.13. The scalable antenna array during measurements in an anechoic chamber.

for each Butler matrix port. During each measurements only one Butler matrix's port was connected to the VNA, whereas, to other ports, the $50\ \Omega$ loads were connected. To measure antenna array's radiation pattern, the antenna array was rotated on the robotic arm with a constant 1° step and for each step transmission between the first and second VNA port was measured.

The measured radiation patterns of the developed multibeam scalable antenna array are shown in Fig. 3.14. As it is observed good radiation properties were achieved and the measured radiation patterns are in a good agreement, apart from the sidelobe level, with the calculated ones. The beams are stable in the $2 - 4$ GHz frequency range, since the HPBW variation is not greater than $\pm 4^\circ$ for 1L&1R beams and $\pm 6^\circ$ for 2L&2R beams, whereas the variations in beams' directions are not greater than $\pm 4^\circ$ for 1L&1R beams and $\pm 2.5^\circ$ for 2L&2R beams, respectively. Although, the measured sidelobe level is higher than the calculated one, it is acceptable and results from the coupling between adjacent radiating elements. The effect of the coupling between the radiating elements was not taken into account in the theoretical analysis, hence, the discrepancies in sidelobe levels are observed. As seen, the measurements confirm the applicability and correctness of the developed concept of multibeam scalable antenna arrays.

3.4.2. 12-element array

The concept of scalable antenna arrays discussed in this subsection is shown in Fig. 3.15. Similarly to the eight element antenna array, the whole antenna array is composed of two centered subarrays. However, in this case, the subarrays are not electrically similar at the lower and higher frequencies ($f_l = f_0$ and $f_h = 2f_0$). As seen the radiating elements operating at higher frequency (red elements) are evenly spaced, whereas elements operating at lower frequency (blue elements) are not. The distance between the red elements d is equal to $0.5\ \lambda$ at higher frequency. Moreover, the distance between the

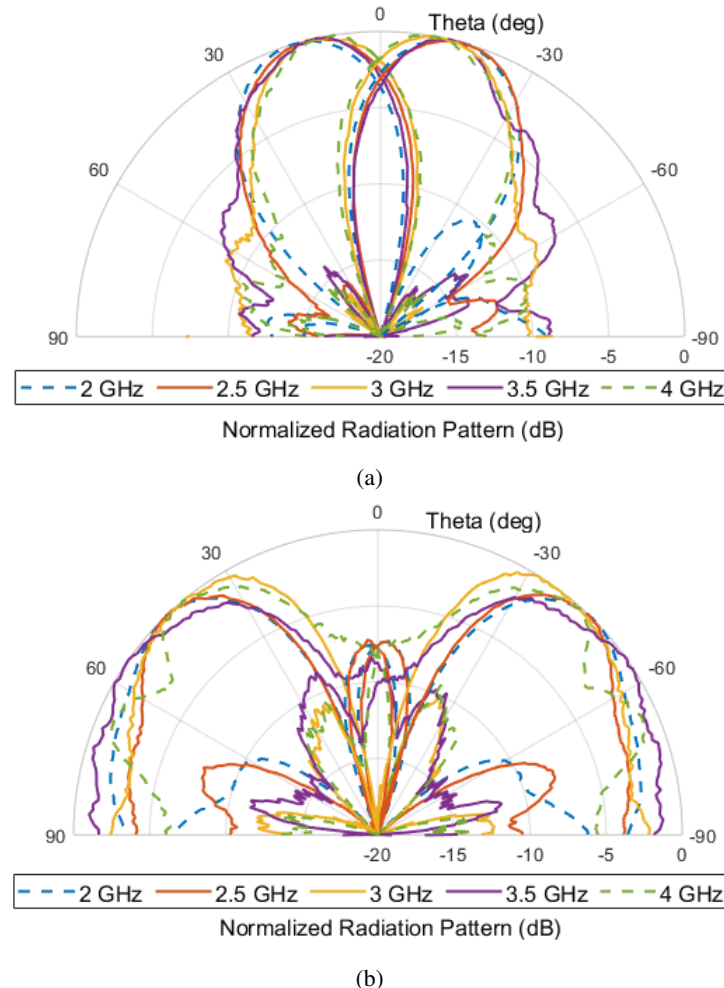


Fig. 3.14. Measured 1L&1R beam (a) and 2L&2R beam (b) radiation patterns for the scalable antenna array depicted in Fig. 3.10 with lossy network.

outer blue elements and adjacent inner ones is also equal to d . On the other hand, the distance between the inner blue elements is two times greater and equal to $2d$. As seen the outer elements in both subarrays are rotated by 180° , which will be explained further.

Such a scalable antenna array is fed by a feeding network composed of a broadband 4×4 Butler matrix, six directional filters, and two unequal power dividers. The utilized Butler matrix is responsible for the phase shift of the signal between pairs of radiating elements, whereas the directional filters realize the signal switching between the elements in each pair. Moreover, the unequal power dividers that realize division in the ratio 1 : 2.6 are utilized to ensure nonuniform amplitude distribution across the antenna array.

Since the Butler matrix has only four outputs and there are six pairs of radiating elements, the outer pairs of elements have to be rotated and fed from the opposite outputs of Butler matrix to ensure constant phase shift. To explain the rotation of radiating elements, all required phase shifts between the pairs of radiating elements are considered in Table 3.5. The phase shifts shown for pairs 2, 3, 4, and 5 are the

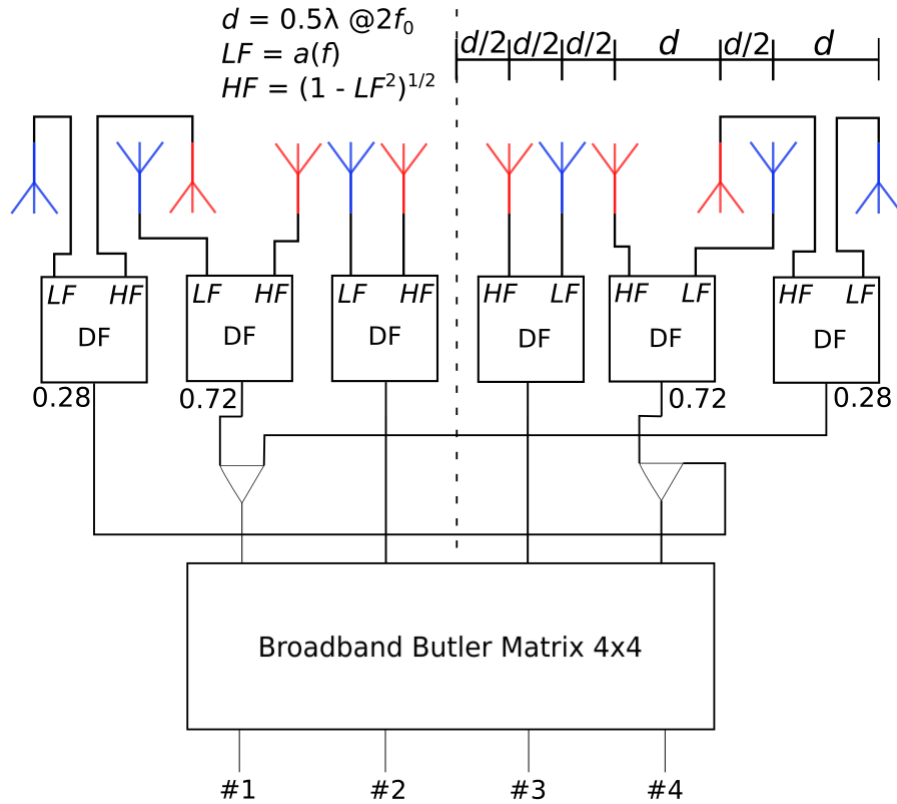


Fig. 3.15. Concept of a twelve-element four-beam scalable antenna array.

phase shifts between the outputs of the Butler matrix. As seen the signal phase delivered to the first pair of radiating elements is always equal to the signal phase delivered to the fifth pair shifted by 180° . Similar dependence is observed between the signal delivered to the sixth pair and the second pair. Therefore, to achieve constant phase shift, signal from the first output should be delivered to the second and sixth pairs of radiating elements and signal from the fourth output should be delivered to the first and fifth pair. Moreover, the signals delivered to the first and sixth pairs should be shifted by 180° . To achieve that phase shifters can be used, however much simpler approach can be utilized since the rotation of radiating elements by 180° introduces ideal 180° phase shift.

The presented multibeam scalable antenna array was analyzed theoretically and the resulting calculated radiation patterns are shown in Fig. 3.16. As seen the 1L&1R beams are stable across the one-octave frequency range. More variation is seen in the 2L&2R beams. Such variation has two causes. First, it is more difficult to maintain more tilted beams constant in the broad frequency range since radiating elements features greater variation of radiation pattern at more tilted angles as the frequency changes. Second, the antenna array is composed of subarrays which are not electrically similar at lower and higher frequency, therefore it is impossible to maintain almost constant radiation pattern across the entire frequency range. However, the utilization of the electrically similar subarrays would result in worse radiation patterns since the grating lobe would appear. Therefore, the utilized placement of radiating elements is optimal.

The scalable antenna array was assembled with the feeding network and measured in an anechoic chamber. Similarly to the aforementioned eight-element antenna array, the same radiating elements, directional filters, and Butler matrix were utilized. The measured radiation patterns are shown in Fig. 3.17. As it is observed good radiation properties were achieved and the measured radiation patterns are in a good agreement with the calculated ones. The HPBW variation is not greater than $\pm 4^\circ$ for 1L&1R beams and $\pm 18^\circ$ for 2L&2R beams, whereas the variations in beams' directions are not greater than $\pm 2.5^\circ$ for 1L&1R beams and $\pm 7^\circ$ for 2L&2R beams, respectively. As seen, the measurements confirm the applicability and correctness of the developed concept of multibeam scalable antenna array.

TABLE 3.5. Phase of the signals fed to the pairs of radiating elements in the antenna array shown in Fig. 3.15.

Phase shift	Pair 1	Pair 2	Pair 3	Pair 4	Pair 5	Pair 6
45°	315°	0°	45°	90°	135°	180°
	$135^\circ - 180^\circ$	0°	45°	90°	135°	$0^\circ - 180^\circ$
-45°	45°	0°	315°	270°	225°	180°
	$225^\circ - 180^\circ$	0°	315°	270°	225°	$0^\circ - 180^\circ$
135°	225°	0°	135°	270°	45°	180°
	$45^\circ - 180^\circ$	0°	135°	270°	45°	$0^\circ - 180^\circ$
-135°	135°	0°	225°	90°	315°	180°
	$315^\circ - 180^\circ$	0°	225°	90°	315°	$0^\circ - 180^\circ$

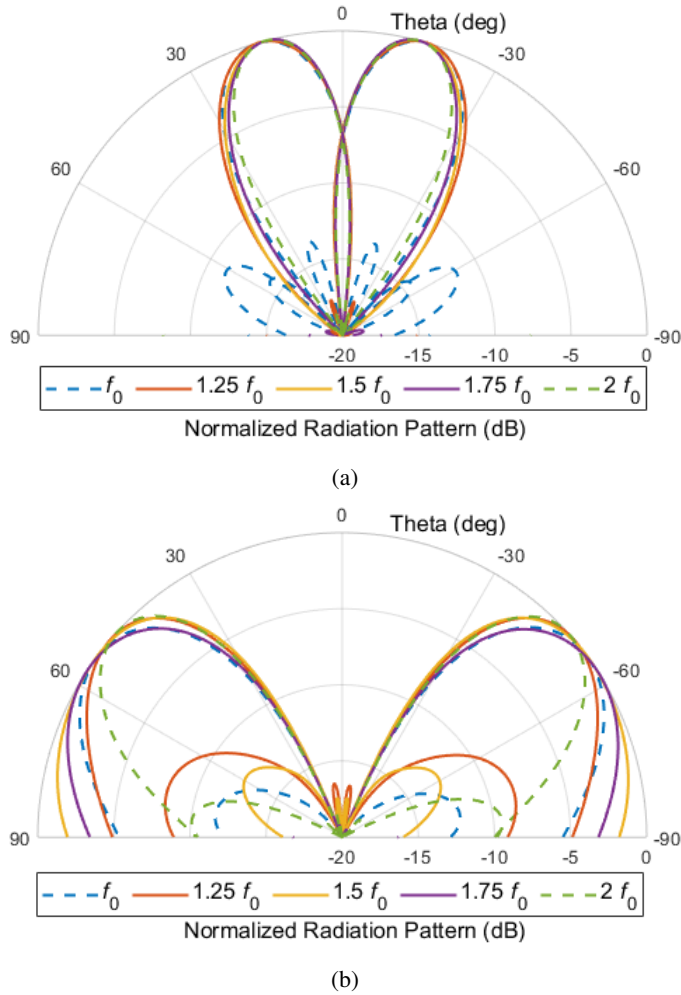


Fig. 3.16. Calculated 1L&1R beams (a) and 2L&2R beams (b) radiation patterns for the scalable antenna array depicted in Fig. 3.15. For calculations the simulated radiation pattern of the antenna element described in Section 3.1 was assumed.

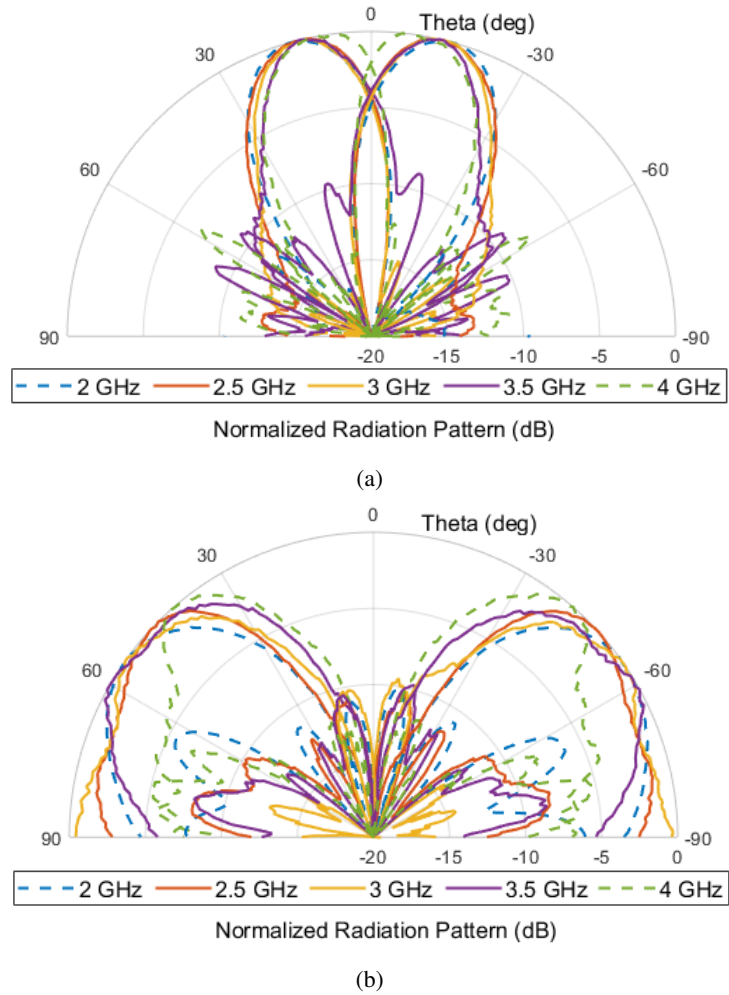


Fig. 3.17. Measured 1L&1R beams (a) and 2L&2R beams (b) radiation patterns for the scalable antenna array depicted in Fig. 3.15.

3.5. Three-beam antennas

In this Section, concepts of three-beam scalable antenna arrays are discussed starting from the five-element array fed by a 3×3 Butler matrix. Moreover, in the following subsections, the antenna arrays with feeding networks based on 4×4 Butler matrix that allows for obtaining 0° , $\pm 90^\circ$, and 180° phase shifts are presented. The discussed three-beam scalable antenna arrays are the subject of two conference papers [16] and [17].

3.5.1. 5-element array

This chapter discusses the concept of a three-beam antenna array with a stable direction of radiation and half-power beamwidth in a broadband frequency range. The concept of the discussed array is represented schematically in 3.18. The presented antenna array consists of three subarrays. Radiating elements in subarrays are deployed at the distance of 0.5λ at a lower frequency f_l (blue elements), whereas the second subarray (red elements) is deployed at a distance of 0.5λ at a higher frequency $f_h = 2f_l$. The third subarray (black element) is centered and belongs simultaneously to the two mentioned subarrays. The distance between the black element and red ones is equal to 0.5λ at a lower frequency. Furthermore, the distance between black and blue elements is equal to 0.5λ at a higher frequency.

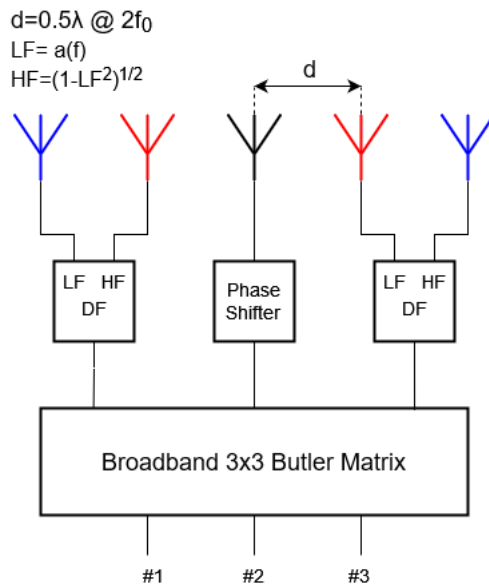


Fig. 3.18. Concept of five-element three-beam scalable antenna array.

The proposed antenna array is fed by broadband 3×3 Butler matrix optimized for frequency 2.5–3.5GHz, which ensures -120° , $+120^\circ$, and 0° differential phase of the signals measured between outputs ports and equal power split for each port. The directional filters connected to the Butler matrix constitute a frequency-selective network providing frequency-domain signal switching between blues and reds elements to obtain satisfying radiation patterns with reduced sidelobe level, constant radiation direction, and half-power beamwidth. It should be emphasized that the middle radiating element operates

with constant excitation in the whole frequency range, which means it radiates exactly the same in both red and blue subarrays.

The proposed concept of a scalable antenna array was analyzed theoretically, and the obtained radiation patterns are shown in 3.19. The antenna array fed by Butler matrix, directional filters and phase shifter allows for expected radiation patterns in an one-octave frequency range. Directions of beams are located at -41° , 0° , 41° . Half-power beamwidth are almost constant for each beam in each of three radiation directions.

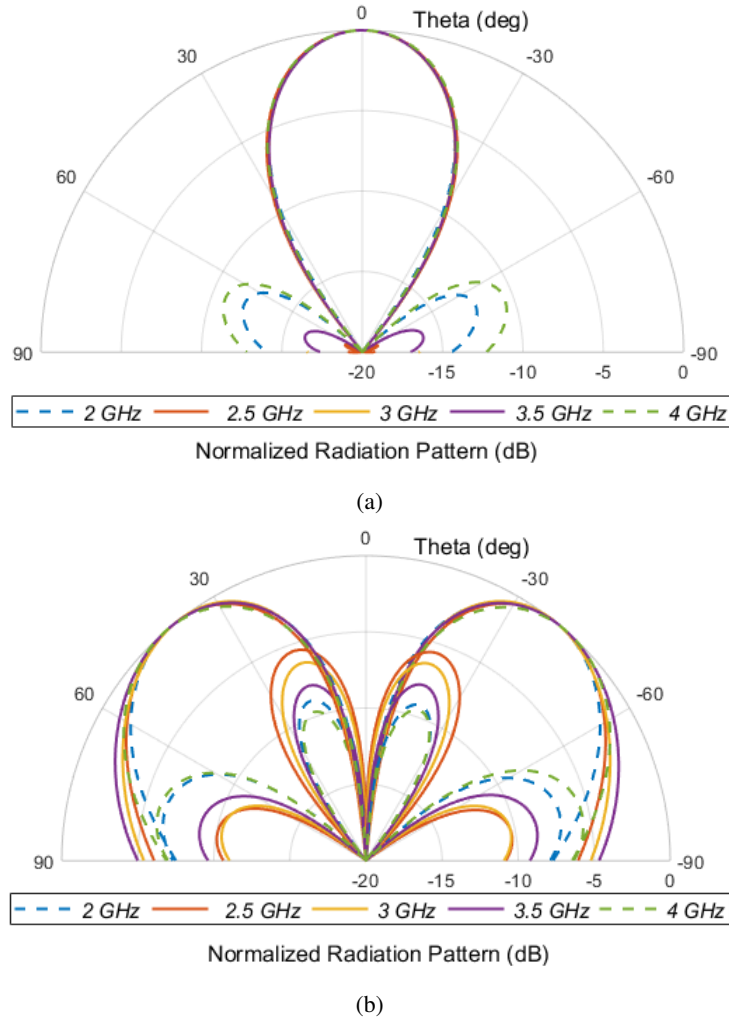


Fig. 3.19. Calculated broadside beam (a) and 1L&1R beams (b) radiation patterns for the scalable antenna array depicted in Fig. 3.18. For calculations the simulated radiation pattern of the antenna element described in Section 3.1 was assumed.

Moreover, beams sidelobe level is acceptable, especially for broadside direction. However, sidelobe levels for 1L1R are noticeably higher, and it is well-known dependence. It is known when the phase progression between the radiating elements increases, the direction of the radiation deviates towards the end-fire, and the level of the side lobes increases. Furthermore, this phenomenon is intensified by the relatively small number of radiating elements used in each antenna subarrays.

The developed scalable antenna array and the feeding network were assembled and measured in an anechoic chamber. The radiation patterns of the antenna array were measured across the operating frequency range for five discrete frequencies as seen in Fig. 3.20.

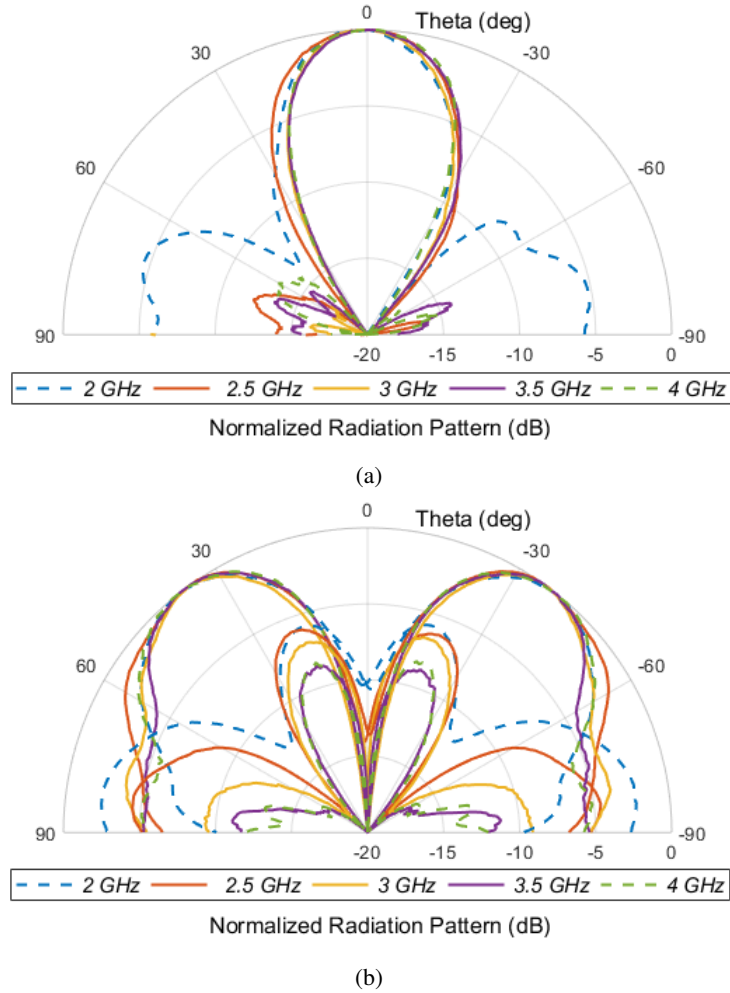


Fig. 3.20. Measured broadside beam (a) and 1L&1R beams (b) radiation patterns for the scalable antenna array depicted in Fig. 3.18.

The theoretical and measured results are in good agreement. The achieved beamwidth variation is not higher than $\pm 4^\circ$, the position of three beams are similar for both calculations and measurements. However, the measured results are satisfying in narrower band, when compared to the calculated results. It is due to the fact the 3×3 Butler matrix was optimized to 2.5–3.5 GHz frequency range, and does not ensure an appropriate performance at lower frequencies of the analyzed bandwidth.

3.5.2. 8-element array

The concept of the three-beam scalable antenna array discussed in this subsection is presented in Fig. 3.21. As seen the scalable antenna array is composed of two centered subarrays. One of the subarrays operates at lower frequency f_l , whereas the other one operates at higher frequency $f_h = 2f_l$. The distance between the radiating elements operating at higher frequency (red elements) is equal to 0.45λ at f_h and the distance between elements operating at lower frequency (blue elements) is equal to 0.45λ at f_l . The array is fed by a feeding network composed of a Broadband 4×4 Butler matrix to which outputs

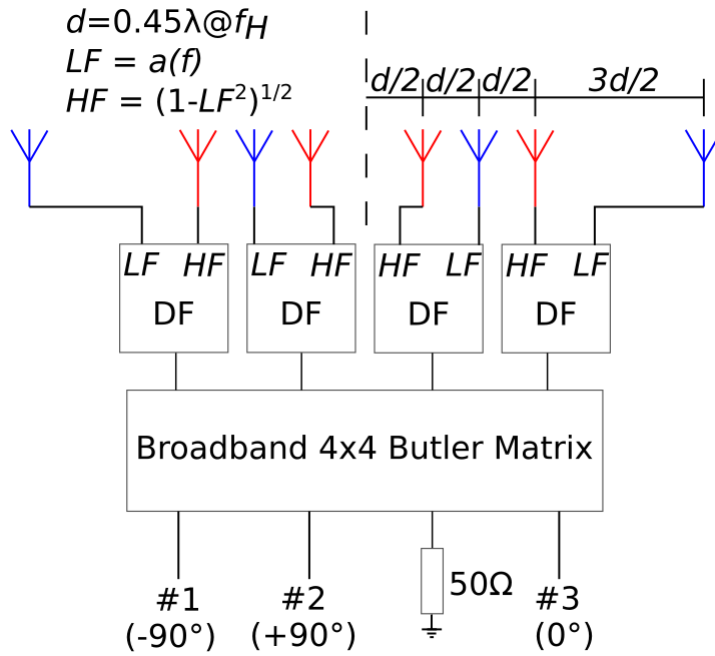


Fig. 3.21. Concept of an eight-element three-beam scalable antenna array.

directional filters are connected. The Butler Matrix, based on [21], utilizes two types of couplers, namely the 3.3 dB $0^\circ/180^\circ$ and 3 dB quadrature couplers. The utilization of such couplers allows for obtaining 0° , $\pm 90^\circ$, and 180° phase shifts, whereas the 4×4 Butler matrix composed of only 3 dB quadrature couplers allows for obtaining $\pm 45^\circ$ and $\pm 135^\circ$ phase shifts. Therefore, the antenna array fed by such a Butler matrix will feature three-beam radiation pattern instead of a four-beam radiation pattern. It results from the fact that 180° phase shift is not used since the resulting radiation pattern will feature 2 end-fire beams (pointing at 90° and -90°). To prevent the utilization of the 180° phase shift one input port of the Butler matrix is connected to 50Ω load. The Butler matrix ensures phase shifts between the

pairs of radiating elements, whereas the directional filters, described in Section 3.2, are responsible for gradual signal switching between elements in each pair. Therefore, such an antenna array can operate in one-octave frequency range.

The idea behind the discussed scalable antenna array cannot be explained without showing the radiation patterns presented in Fig. 3.22. As seen there are no sidelobes having maximum radiation for 0° and the sidelobe level is below -10 dB. Therefore, there is no need to utilize lossy feeding network in the discussed antenna array. It is due to the lesser deflections of 1L&1R beams than the deflections of 2L&2R beams in case of the scalable antenna array presented in Subsection 3.4.1. Moreover, the calculated radiation pattern features little variation in beam direction and HPBW. For the broadside beam the

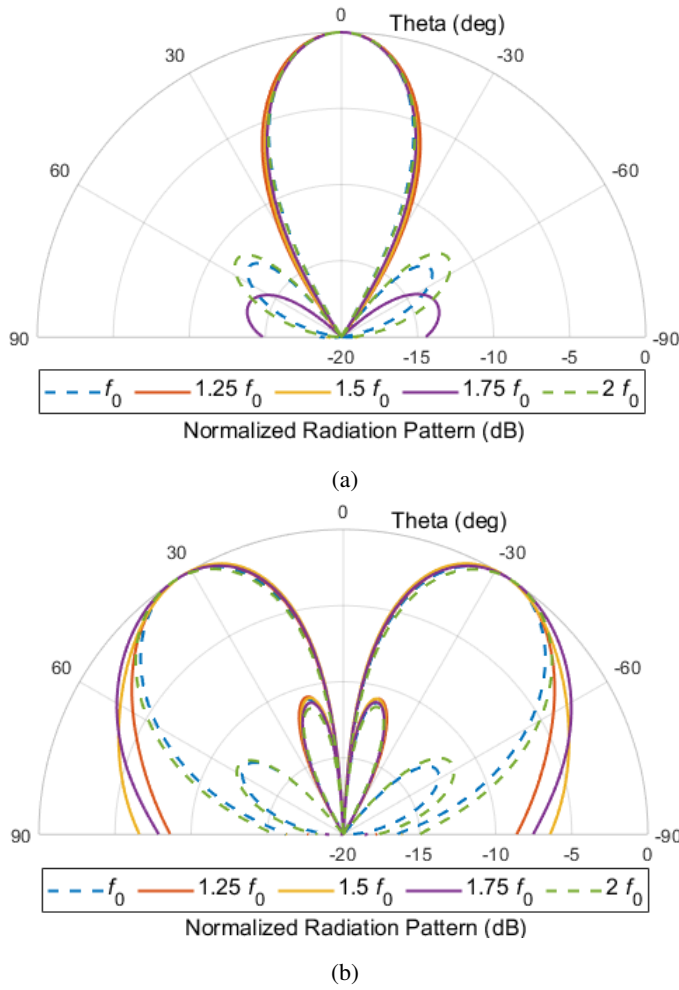


Fig. 3.22. Calculated broadside beam (a) and 1L&1R beams (b) radiation patterns for the scalable antenna array depicted in Fig. 3.21. For calculations the simulated radiation pattern of the antenna element described in Section 3.1 was assumed.

variation in beam's direction is not observed, whereas for 1L&1R beams the variation does not exceed the $\pm 1.5^\circ$. The observed HPBWs are also stable and their variations are not greater than $\pm 1^\circ$ and $\pm 5^\circ$ for broadside beam and 1L&1R beams, respectively.

The antenna array with the described feeding network was assembled. Similarly to other antenna arrays described in this Chapter, the same radiating elements and directional filters were utilized. Moreover, the Butler Matrix described in [21] was used since its operational frequency range covered the desired 2 – 4 GHz frequency range. The antenna array was measured in an anechoic chamber in the same way as all multibeam scalable antenna arrays. Fig. 3.23 presents the resulting radiation patterns measured at five uniformly spaced frequencies in the 2 – 4 GHz frequency range. As seen the resulting beams are stable in

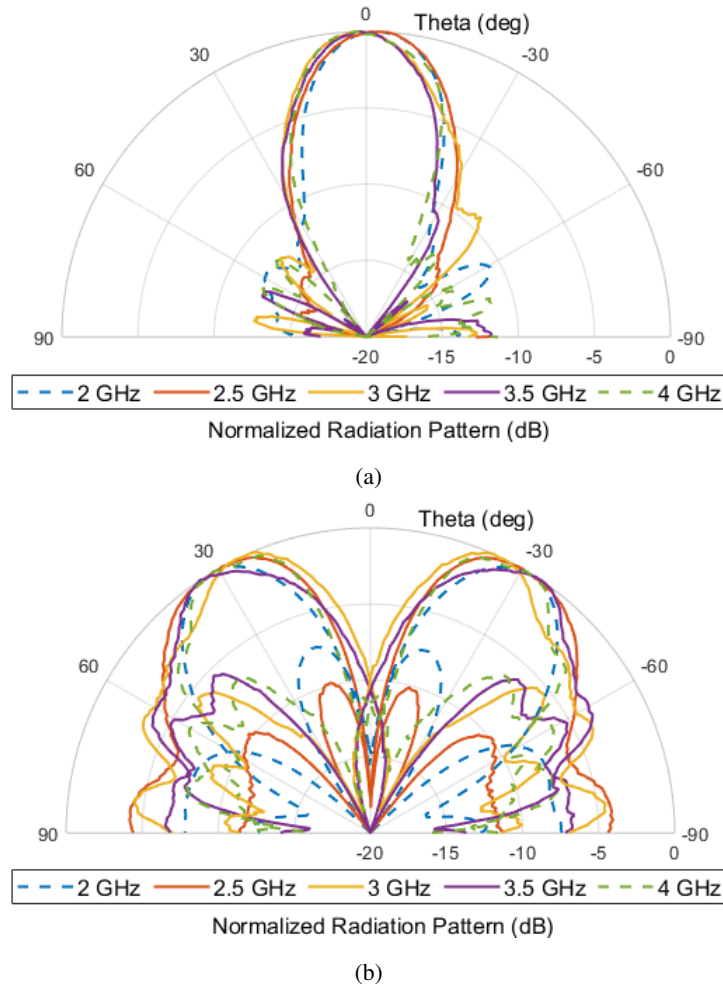


Fig. 3.23. Measured broadside beam (a) and 1L&1R beam (b) radiation patterns for the scalable antenna array depicted in Fig. 3.21.

the entire frequency range, however slight variations of all beams' directions and HPBWs are observed. The HPBWs variations do not exceed $\pm 2^\circ$ for broadside beam and $\pm 4.5^\circ$ for 1L&1R beams, whereas the variations of beam directions are not greater than $\pm 3^\circ$ for broadside beam and $\pm 4^\circ$ for 1L&1R beams, respectively. Although, the measured sidelobe level is greater than the calculated one, it is acceptable. The root cause of the discrepancy between the calculated radiation patterns and the measured ones is the mutual coupling between adjacent radiating elements. The obtained measurements confirm the correctness of the presented concept and design of three-beam scalable antenna arrays.

3.5.3. 12-element array

The scalable antenna arrays discussed in this Subsection are similar to the array described in Subsection 3.4.2 and their concepts are shown in Fig. 3.24. The similarity is seen in the placement of the radiating elements since their positions are exactly the same. In the first concept (Fig. 3.24a), the same rotation of the radiating elements, as the one discussed in Subsection 3.4.2, was utilized. However, as seen in Fig. 3.24b, the rotation of the radiating elements is not necessary, which is explained further. Moreover, a similar feeding network is utilized in these scalable antenna arrays since the same directional filters and power dividers are used. The difference in the feeding network is the utilized Butler matrix. In the feeding network described in the Subsection 3.4.2, a conventional 4×4 Butler matrix that ensures $\pm 45^\circ$ and $\pm 135^\circ$ phase shifts is used. On the other hand, in this concept a 4×4 Butler matrix that ensures 0° , $\pm 90^\circ$, and 180° phase shifts is utilized. Similar Butler matrix was used in the feeding network of the antenna array described in Subsection 3.5.2.

Due to the utilization of a Butler matrix which ensures 0° , $\pm 90^\circ$, and 180° phase shifts, it is not necessary to rotate the radiating elements in the outer pairs. Such an approach is shown in Fig. 3.24b, whereas the rotation of the radiating elements in the outer pairs is utilized in the scalable antenna arrays presented in Fig. 3.24a and described in Subsection 3.4.2. As a result, in the antenna array shown in Fig. 3.24b, a constant phase progression between the pairs of radiating elements is achieved, whereas phase progression achieved between the pairs of elements in the antenna array shown in Fig. 3.24a is not constant. The constant phase progression is explained in Table 3.6 where phase shifts shown for pairs 2, 3, 4, and 5 are the phase shifts between the outputs of the utilized Butler matrix. As seen pair 1 and pair 5 should be fed with the signals having the same phase. Similarly, pair 2 and 6 should be fed with the in-phase signals. Although, the phase progression between the pairs of radiating elements in the antenna array shown in Fig. 3.24a is not constant, it has to be underlined that such a phase progression does not make it impossible to develop an antenna array featuring stable radiation pattern.

TABLE 3.6. Phase of the signals fed to the pairs of radiating elements in the antenna array shown in Fig. 3.24b.

Phase shift	Pair 1	Pair 2	Pair 3	Pair 4	Pair 5	Pair 6
90°	270°	0°	90°	180°	270°	0°
-90°	90°	0°	270°	180°	90°	0°
0°	0°	0°	0°	0°	0°	0°

Both scalable antenna arrays were analyzed theoretically. For simplicity, only the radiation patterns calculated for the antenna array presented in Fig. 3.24b are shown in Fig. 3.25. As seen the broadside beam radiation pattern is stable in an one-octave frequency range, whereas the 1L&1R beams feature slight variation. However, it has to be underlined that variation in 1L&1R beams is expected since the scalable antenna array is composed of two subarrays that are not electrically similar at lower and higher

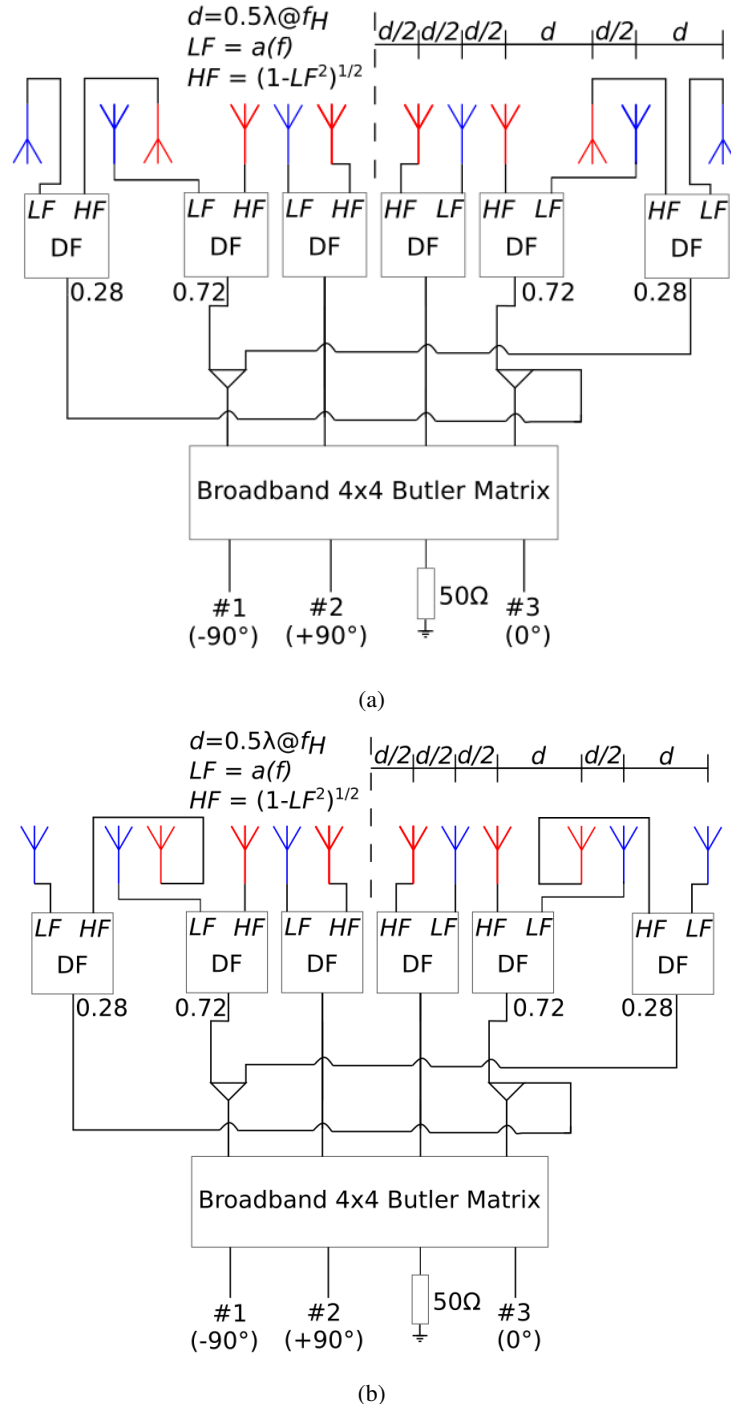


Fig. 3.24. Concept of a twelve-element three-beam scalable antenna array presented in [16] (a) and corrected concept of a twelve-element three-beam scalable antenna array (b).

frequencies ($f_l = f_0$ and $f_h = 2f_0$). Moreover, this variation is reduced compared to the variation of beams shown in Fig. 3.16b. It is due to the lesser beam deflection which results from the application of smaller phase progression between the pairs of radiating elements.

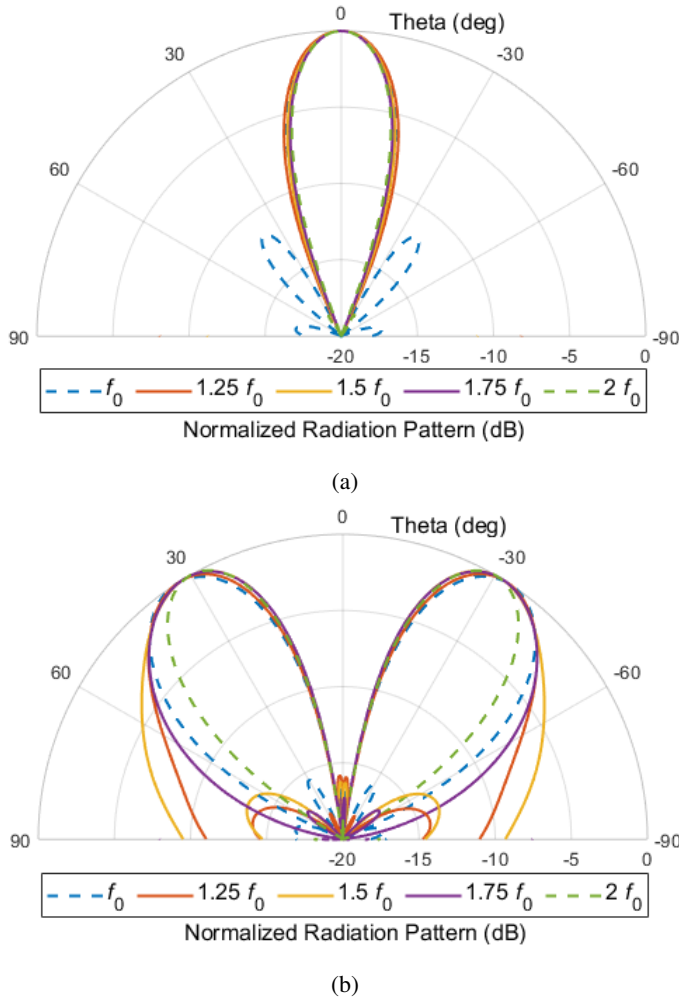


Fig. 3.25. Calculated broadside beam (a) and 1L&1R beams (b) radiation patterns for the scalable antenna array depicted in Fig. 3.24b. For calculations the simulated radiation pattern of the antenna element described in Section 3.1 was assumed.

The scalable antenna arrays with a corresponding feeding networks were assembled and measured in an anechoic chamber. The resulting radiation patterns are shown in Fig. 3.26 and Fig. 3.27. As seen the resulting broadside beams are stable in the entire frequency range and the 1L&1R beams feature the predicted variation. Moreover, slight variations of all beams' directions and HPBWs are observed. First, the results for the antenna array that is shown in Fig. 3.24a, are considered. The HPBWs variations do not exceed $\pm 4^\circ$ for broadside beam and $\pm 3.5^\circ$ for 1L&1R beams, whereas the variations of beam directions are not greater than $\pm 2.5^\circ$ for broadside beam and $\pm 4^\circ$ for 1L&1R beams, respectively. Second, the results for the antenna array that is presented in Fig. 3.24b, are discussed. The HPBWs variations do not exceed $\pm 3^\circ$ for broadside beam and $\pm 5^\circ$ for 1L&1R beams, whereas the variations of beam directions are not greater than $\pm 2.5^\circ$ for broadside beam and $\pm 3^\circ$ for 1L&1R beams, respectively. As seen the measurements confirm the correctness of the described approaches to develop three-beam scalable antenna arrays.

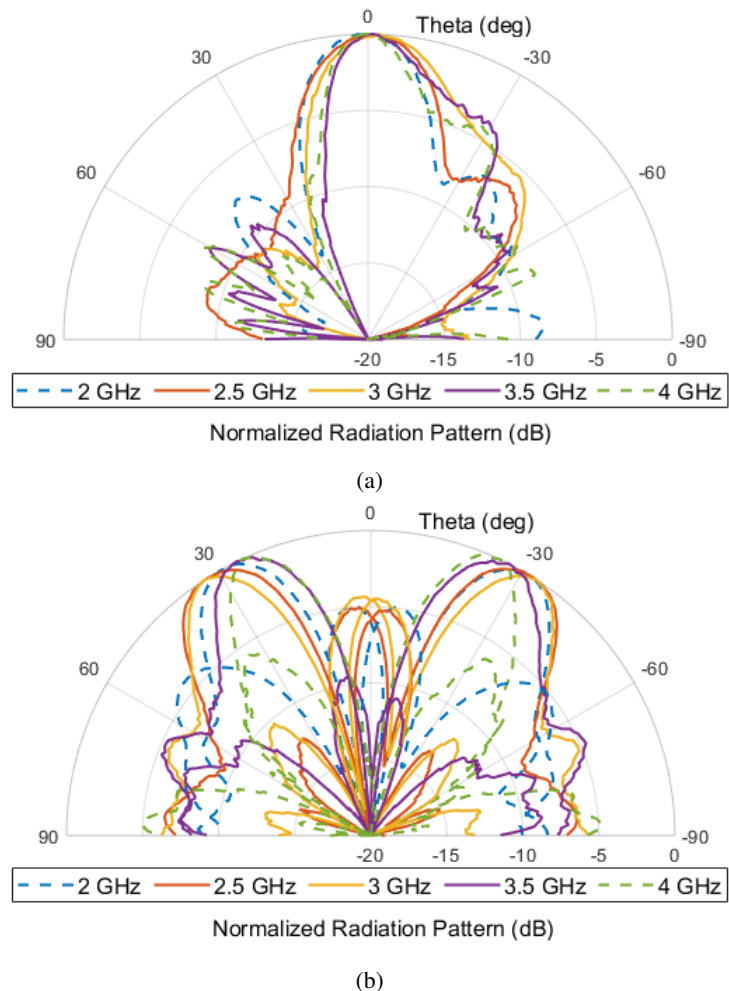


Fig. 3.26. Measured broadside beam (a) and 1L&1R beams (b) radiation patterns for the scalable antenna array depicted in Fig. 3.24a.

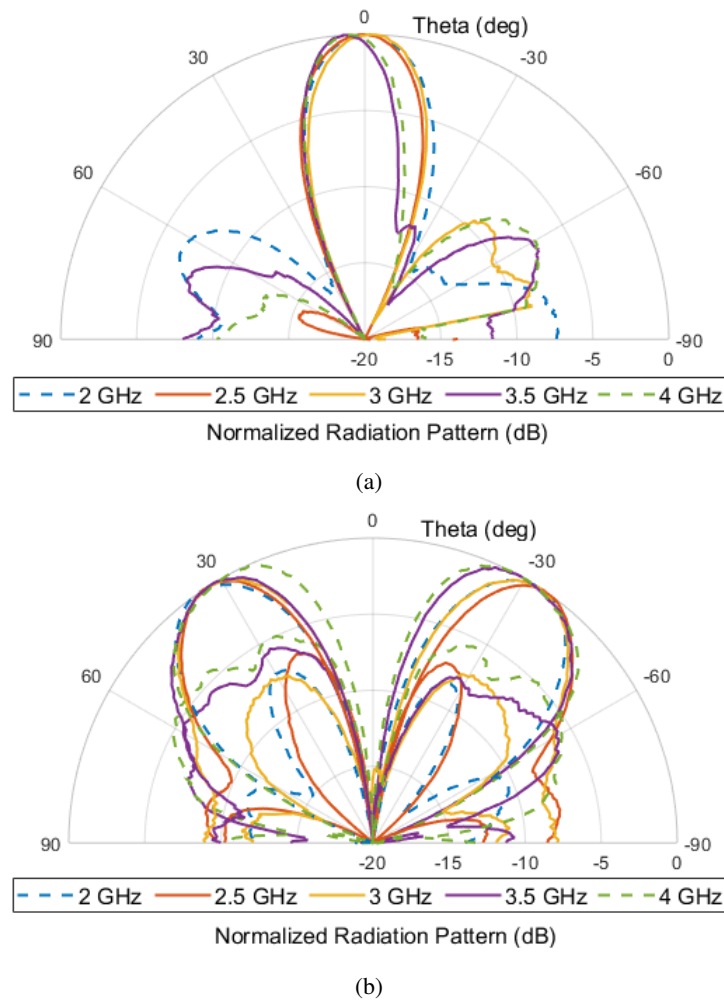


Fig. 3.27. Measured broadside beam (a) and 1L&1R beams (b) radiation patterns for the scalable antenna array depicted in Fig. 3.24b.

4. Broadside beam scalable antenna array

In this Chapter, the developed two-octave broadside beam scalable antenna array is discussed. The presented antenna array is based on a developed concept to realize multi octave scalable antenna arrays which is presented and explained in the following subsections. First, the placement of the radiating elements and utilization of signal switching are analyzed and followed by the review of a physically realized elements of the scalable antenna array and feeding network. The Chapter is summarized by the comparison of the theoretical and measured results. The presented concept and developed antenna array were the subject of the submitted article [18].

4.1. Concept of a broadside beam scalable antenna array

The concept of scalable antenna arrays presented in this Chapter aims at extending, theoretically to infinity, the operational BW of the antenna array. Moreover, such a concept allows for a theoretical infinite increase of the even number of radiating elements. To summarize, such antenna arrays can operate over $R^N : 1$ BW and are composed of $N + 1$ centered $2K$ -elements subarrays where both N and K are arbitrary natural numbers. The concept is presented in the following paragraphs.

According to the theory of scalable antenna arrays, the maximum BW over which a scalable antenna array can operate results from the placement of radiating elements. As it was presented in Fig. 2.6, the distances between radiating elements in one subarray (blue elements) are two times greater than distances between elements in the second subarray (red elements). Such a dependence allows for obtaining a $2 : 1$ BW. To explain such a dependence a scalable antenna array shown in Fig. 4.1 is considered. As seen the antenna array is composed of two two-element subarrays. Signal is switched from the blue elements to the red ones with the frequency increase as it is indicated by the arrows. Moreover, in one subarray, the distance between the radiating elements is equal to d , whereas in the other one the distance between the elements is equal to Rd . Therefore, the maximum BW over which such a scalable antenna array can operate is equal to $R : 1$.

Theoretically it is possible to extend the R to infinity to ensure infinite BW, however it is impossible to develop such a scalable antenna array. Therefore, to extend the operational BW it is possible to divide the BW into subbands and achieve $R^N : 1$ BW. The problem of BW division can be approached in many ways, however two main aspects shall be considered in such analysis. First, the operational BW of a single radiating element has to be taken into account since the wider the subband the wider the BW of

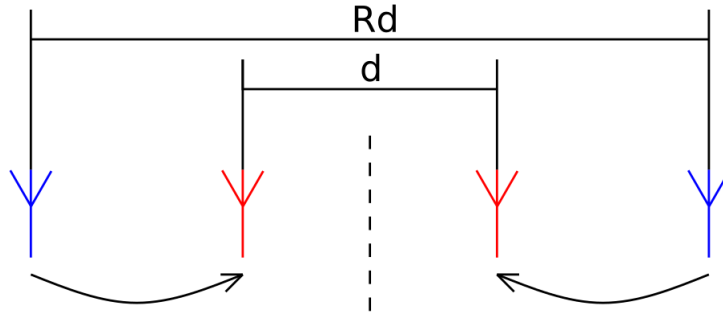


Fig. 4.1. A 4-element scalable antenna array that can theoretically operate over $R : 1$ BW.

element is needed. Second, the placement of the radiating elements is has to be analyzed since the choice of R influences not only the operational BW, but also the arrangement of radiating elements. As it was mentioned the scalable antenna array is composed of $N + 1$ centered $2K$ -elements subarrays. In order to achieve stable radiation pattern across $R^N : 1$ BW the radiating elements in these subarrays have to be placed in such a way that consecutive subarrays from $0, 1, \dots, N$ are electrically similar at consecutive frequencies $R^0 f_0, R^1 f_0, \dots, R^N f_0$. Such an element placement with respect to the center of the scalable antenna array can be given by:

$$|x_{n,k}| = R^{N-n} \frac{d}{2}(2k - 1) \quad (4.1)$$

where:

$x_{n,k}$ – position of radiating element,

n – number of the subarray for which the element placement is calculated (n is in the range from 0 to N),

k – number of the element in the n -th subarray (k is in the range from 1 to K),

R – ratio between the higher and lower frequencies in each subband,

d – distance between radiating elements in the N -th subarray, typically equal to 0.5λ at $R^N f_0$.

The positions of radiating elements were analyzed for different values of R , N , and K . To visualize the analysis, the positions of radiating elements were calculated using (4.1) for $N = 2$, $K = 2$, and R from 1.25 to 3.25 with a 0.25 step and are shown in Fig. 4.2. As seen the selection of R has a significant impact on the placement of radiating elements. On one hand, when R is close to 1 or 3 the radiating elements operating over different subbands are close to each other. Especially it is seen for $R = 3$ where the elements operating over different subbands have the same positions. Therefore, such elements would require greater than $3 : 1$ BW for example 9 : 1 or 27 : 1 etc., depending on the values of N and K . Although, such radiating elements or scalable antenna arrays are not theoretically impossible to develop, their physical realization is hard to implement. On the other hand, when R is equal to 2 or any subsequent even number, the distance between the adjacent radiating elements is maximized and the elements operating in different subbands cannot be placed in the same positions regardless the values of

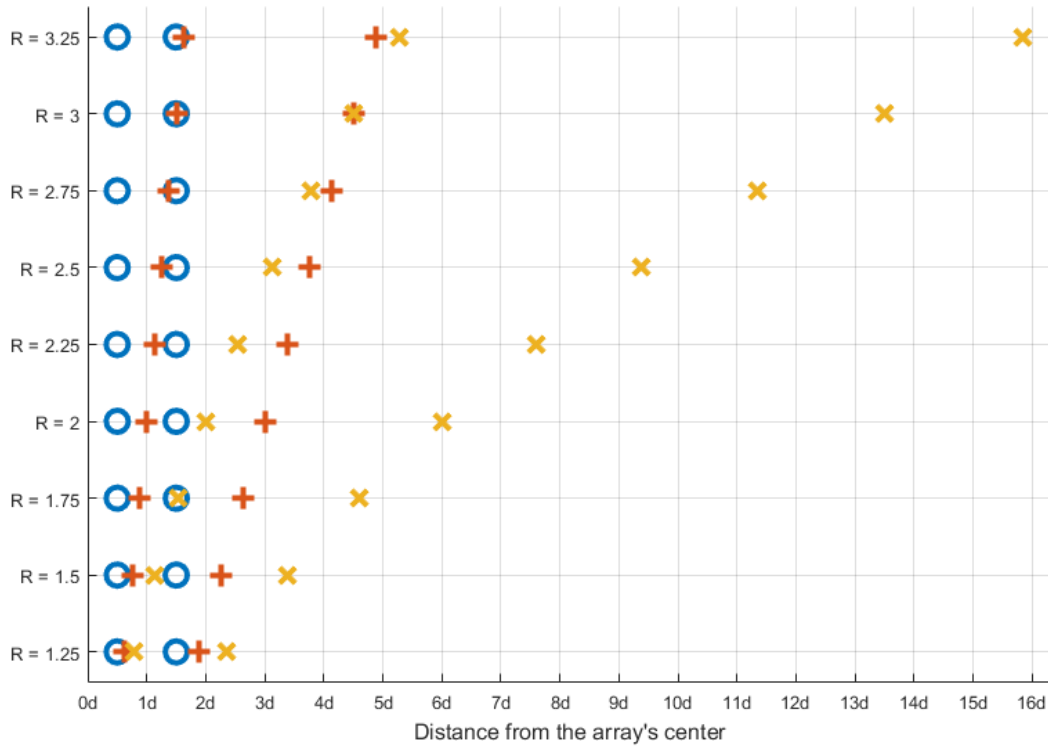


Fig. 4.2. Radiating element positions calculated for an antenna array operating in two subbands ($N = 2$, each subband has $R : 1$ BW) and composed of 12 radiating elements ($K = 2$) vs. different values of R . Only the positive halves of the arrays are shown. Radiating elements from different subarrays are depicted with different symbols.

N and K . Therefore, the use of $R = 2$ is the optimal solution since the distance between the radiating elements is maximized and the required BW of every single radiating element is relatively easy to ensure. As a result, the selection of R equal to 2 allows for realization of scalable antenna arrays featuring stable radiation pattern over theoretically infinite BW (N infinite), composed of subarrays in which an infinite-even number of elements is utilized.

Another important aspect regarding the presented concept is the signal switching between the elements. To visualize these signal switching a scalable antenna array operating in two-octave frequency range is presented in Fig. 4.3. As seen the signal is switched between radiating elements placed at positions having the same sign (positive or negative) and the same k , e.g., signal is switched between elements placed at $x_{0,1}$, $x_{1,1}$, and $x_{2,1}$. Moreover, the signal is switched in such a way that the entire signal is fed to the blue elements at f_0 , green elements at $2f_0$, and red elements at $4f_0$. In the first frequency octave the signal is gradually switched from blue elements to the green ones and the red ones do not receive any signal, whereas the signal is switched from the green elements to the red ones and blue ones do not receive any signal in the second frequency octave. According to the model of virtual radiating

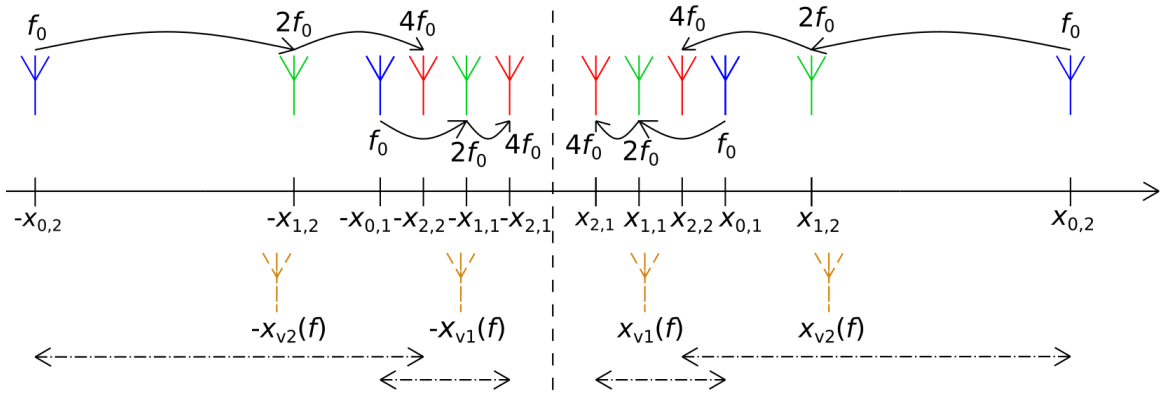


Fig. 4.3. A twelve-element scalable antenna array operating over two-octave BW ($N = 2, K = 2$) with arrows indicating signal switching between the elements and a corresponding four-element virtual antenna array having frequency-dependent positions.

element, such a twelve element array can be viewed as a four-element array having frequency-dependent positions. These four elements are placed in $-x_{0,2}$, $-x_{0,1}$, $x_{0,1}$, and $x_{0,2}$ at f_0 . With the frequency increase these elements are shifted to the corresponding positions $-x_{1,2}$, $-x_{1,1}$, $x_{1,1}$, and $x_{1,2}$ at $2f_0$ and finally to $-x_{2,2}$, $-x_{2,1}$, $x_{2,1}$, and $x_{2,2}$ at $4f_0$. In general, at any given frequency equal to $2^n f_0$ the entire signal is fed only to the elements of one n -th subarray, whereas in the frequency octave between such two consecutive frequencies e.g., $2^n f_0$ and $2^{n+1} f_0$, the signal is switched from the radiating elements of n -th subarray to the elements of $n + 1$ -th subarray. Moreover, every frequency subband in this case ($R = 2$) is a frequency octave. Therefore, the same switching function, however scaled in frequency, should be used for every frequency octave in the entire frequency range. Furthermore, to derive switching function, according to the model of virtual radiating element, only two elements between which the signal is switched over one frequency octave have to be analyzed. For visualization purposes the set of optimized switching functions, derived with the use of the model of virtual radiating element, for an antenna array operating in 16:1 BW is shown in Fig. 4.4. As seen in each frequency octave switching function presented in Fig. 2.8a is utilized. As a result the achieved AF calculated for the antenna array in which radiating elements are placed according to (4.1) for $R = 2, N = 4, K = 2$, and $d = 0.5\lambda$ at $16f_0$ is exactly the same as the one shown in Fig. 2.8b, as presented in Fig. 4.5.

The last aspect regarding the presented concept of scalable antenna arrays is the utilization of different radiating elements. The common approach in the development of scalable antenna arrays is the use of the same single radiating element in every subarray. This approach limits the possible scalability since the maximum operational BW of the antenna array is not greater than the operational BW of the single radiating element utilized in the array. To overcome this problem it is possible to use radiating elements featuring wider BWs, however that approach has significant drawbacks. First, the radiation pattern of a single radiating element varies with the frequency increase since the aperture of single radiating element is constant and the wavelength decreases. Such relation affects the radiation pattern which is especially seen in the more narrow HPBW at higher frequencies compared to the one observed at lower ones. The

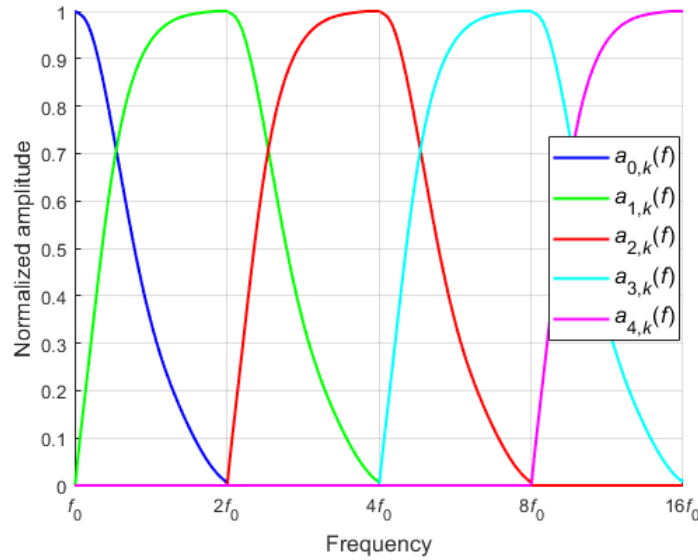


Fig. 4.4. Set of alike switching functions used for signal switching between radiating elements in five subarrays in the four-octave frequency range.

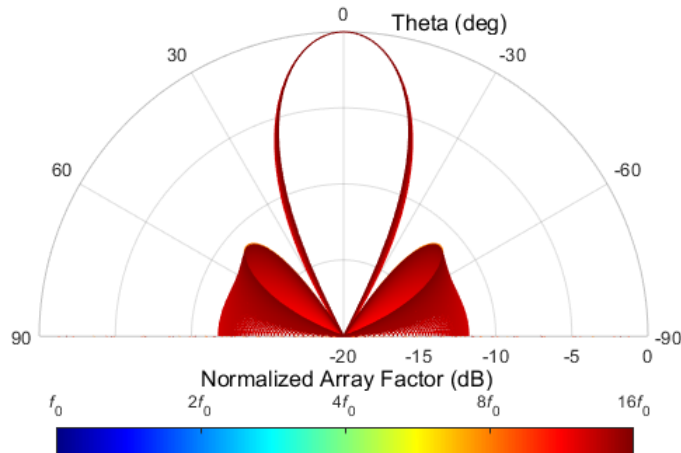


Fig. 4.5. AF calculated for a scalable antenna array composed of 20 radiating elements operating in four-octave frequency range in which elements are placed according to (4.1) for $R = 2$, $N = 4$, $K = 2$, and $d = 0.5\lambda$ at $16f_0$.

variation in HPBW can be reduced and kept acceptable in the one-octave frequency range by proper selection of the radiating element, however it is impossible to maintain stable radiation pattern over wider frequency ranges. The other aspect regarding the broadening of single radiating element's operational BW is connected to the physical dimensions of the element. The wider the BW is required the greater the physical dimensions since the dimensions of the single radiating element are closely related to the wavelength at the lowest operational frequency. As a result the elements having relatively large dimensions cannot be placed close enough to ensure proper operation. To eliminate the aforementioned drawbacks it is possible to utilize different radiating elements in each subarray. This idea is a result of the concept

of BW division since radiating elements in different subarrays receive signal in different parts of the operational BW as seen in Fig. 4.4. As seen the maximum required BW that a single radiating element has to ensure is equal to 4 : 1. However, crossing frequencies at which power is equally split between two subarrays (signal amplitude equal to 0.707) can be distinguished. The subband between two consecutive crossing frequencies is equal to one frequency octave since the same switching function is used in every frequency octave. In this frequency octave between two consecutive crossing frequencies, the signal is mainly fed to only one subarray (signal amplitude greater than 0.707). Therefore, the minimum BW that the single radiating element has to ensure is equal to one frequency octave.

All of the aforementioned ideas i.e., BW division, signal switching, radiating element placement, and use of different radiating elements allow for realization of scalable antenna arrays featuring stable radiation pattern in multi octave (theoretically infinite) BW and composed of theoretically infinite even number of radiating elements. To verify the concept experimentally, the twelve-element antenna array operating in 1.2 – 4.8 GHz frequency range was developed and measured. The schematic diagram of the antenna array with the feeding network is presented in Fig. 4.6. As seen the radiating elements were placed according to (4.1 for $R = 2$, $N = 2$, $K = 2$, and $d = 0.6\lambda$ at 4.8 GHz). The radiating elements are fed by a directional filter to which outputs three identical equal-split power dividers are connected. In the following sections the utilized elements are discussed starting from the directional filter. Moreover, power dividers and radiating elements are presented. The Chapter ends with the discussion of the measured results.

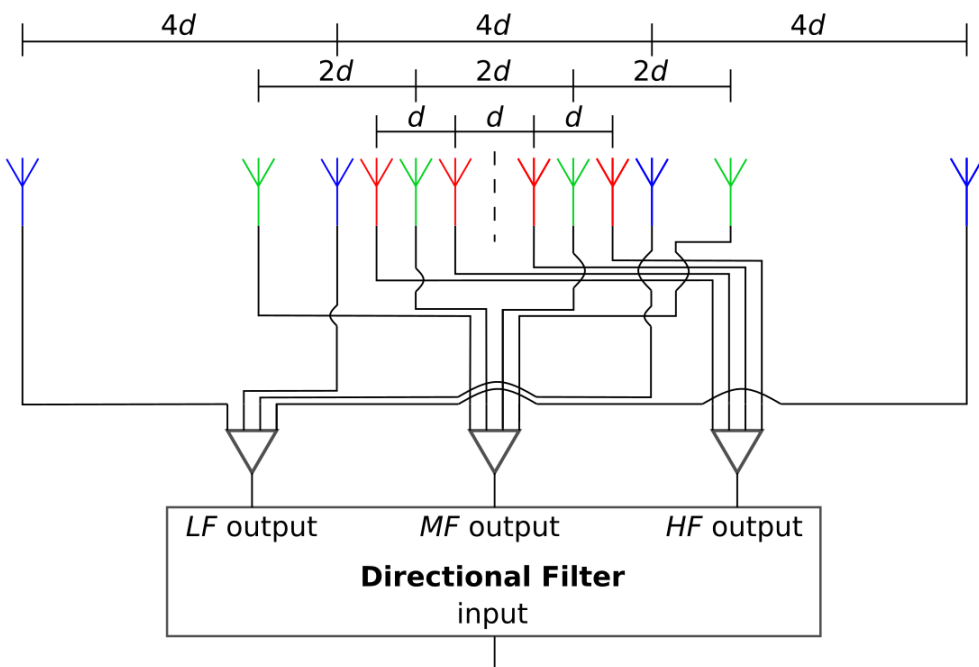


Fig. 4.6. Schematic diagram of the developed two-octave scalable antenna array with the feeding network.

4.2. Directional filter

The principal element of the feeding network is the directional filter that is utilized to ensure proper signal switching between corresponding elements in each subarray. Fig. 4.7a shows the schematic diagram of the directional filter in which two groups of elements having two distinct functions can be distinguished. First, the elements couplers C_A and low-pass filters LPF 1 and LPF 2 are responsible

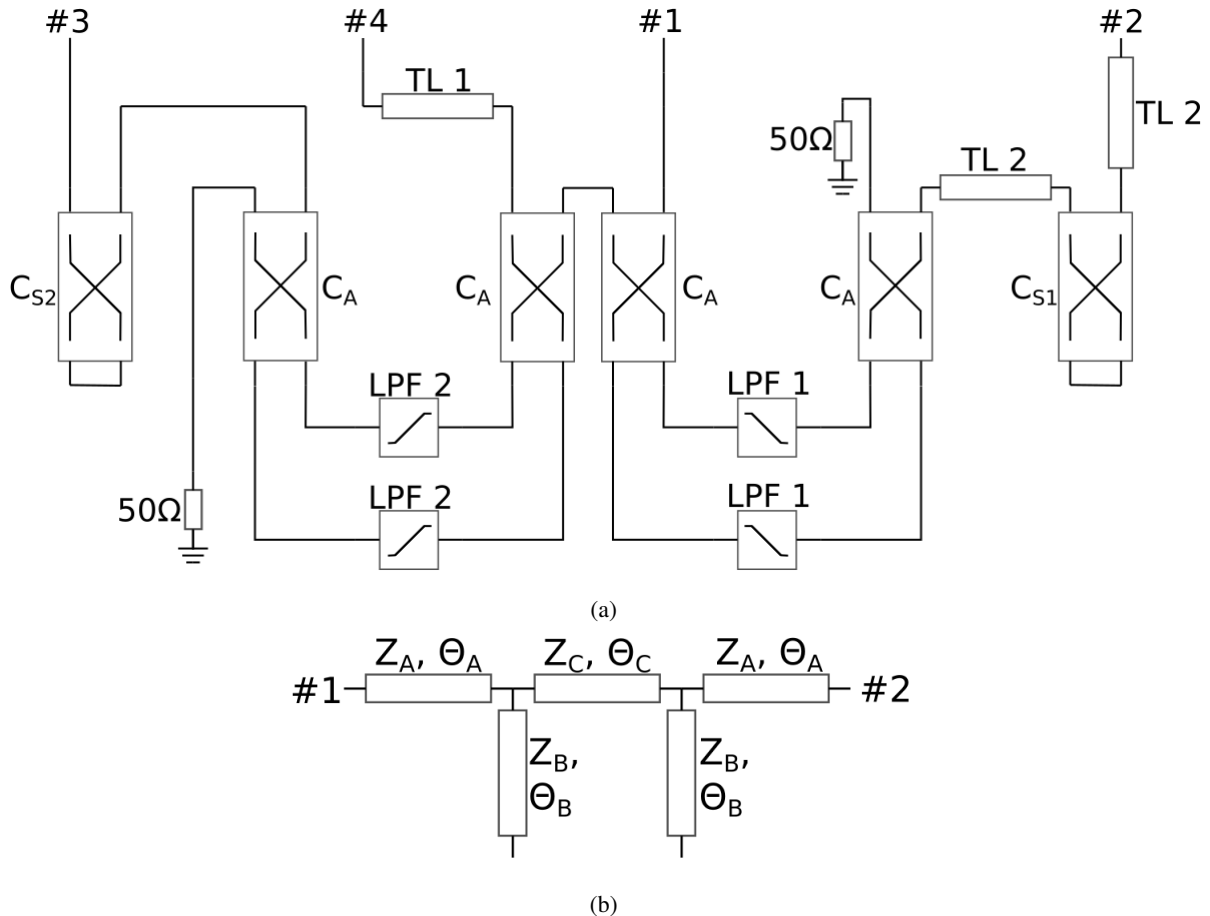


Fig. 4.7. Schematic diagram of the directional filter (a) and schematic diagram of the low pass filters utilized in the directional filter (b).

for the faithful reproduction of the switching function (magnitude part). These elements constitute two octave-band directional filters. Each octave-band directional filter is composed of two couplers C_A and two low-pass filters of the same type (LPF 1 or LPF 2). The directional filter in which LPF 1 low-pass filters are utilized switches the signal in the first frequency octave (1.2 – 2.4 GHz), whereas the other one switches the signal in the second frequency octave (2.4 – 4.8GHz). These two octave-band directional filters are connected in such a way that the high frequency signal, that cannot pass the first one, is fed to the input of the second one. Both low-pass filters are composed of five transmission lines arranged in a way presented in Fig. 4.7b. Moreover, there is a second group of elements responsible for the phase shift of the signal since the signal at the outputs of octave-band directional filters are out of phase. In this

group there are two Schiffman C-sections C_{S1} and C_{S2} , two transmission lines TL 2, and transmission line TL 1. However, it has to be underlined that the signal at all of the outputs of the entire directional filter are not in phase throughout two frequency octaves. It is due to the idea of BW division according to which only two consecutive subarrays are fed in one subband. Therefore, the phase difference between ports 2 and 3 (LF and MF outputs) is kept close to 0° in the first frequency octave, whereas the phase difference between ports 3 and 4 (MF and HF outputs) is kept close to 0° in the second frequency octave.

The electrical parameters of the designed directional filter were thoroughly chosen to closely reproduce the switching function, that is shown in Fig. 2.8a, in two frequency octaves. The electrical parameters of the elements constituting the developed filter, apart from the coupler C_A that is based on [22] are shown in Table 4.1.

TABLE 4.1. Electrical parameters of the developed directional filter.

Element	Parameter	Value
LPF 1	Z_A	100Ω
	Z_B	20Ω
	Z_C	100Ω
	Θ_C	25.35°
	Θ_C	23.38°
	Θ_C	48.81°
LPF 2	Z_A	54.3Ω
	Z_B	58.2Ω
	Z_C	66Ω
	Θ_C	45°
	Θ_C	21.3°
	Θ_C	30.8°
TL 1	Z_1	50Ω
	Θ_1	37.37°
TL 2	Z_2	50Ω
	Θ_2	118.7°
C_{S1}	k_{S1}	0.42
	Θ_{S1}	63.18°
C_{S2}	k_{S2}	0.28
	Θ_{S2}	22.87°

The designed directional filter was realized in a homogeneous symmetric stripline structure in which a thin layer of dielectric laminate having thickness h_2 equal to $50.8 \mu\text{m}$ is inserted between two thick

layers having thickness h_1 equal to 1.52 mm. All the layers have the same dielectric constant equal to 3.38. Fig. 4.8 shows the layout of the designed directional filter and the cross-sectional schematic view of the utilized stripline structure.

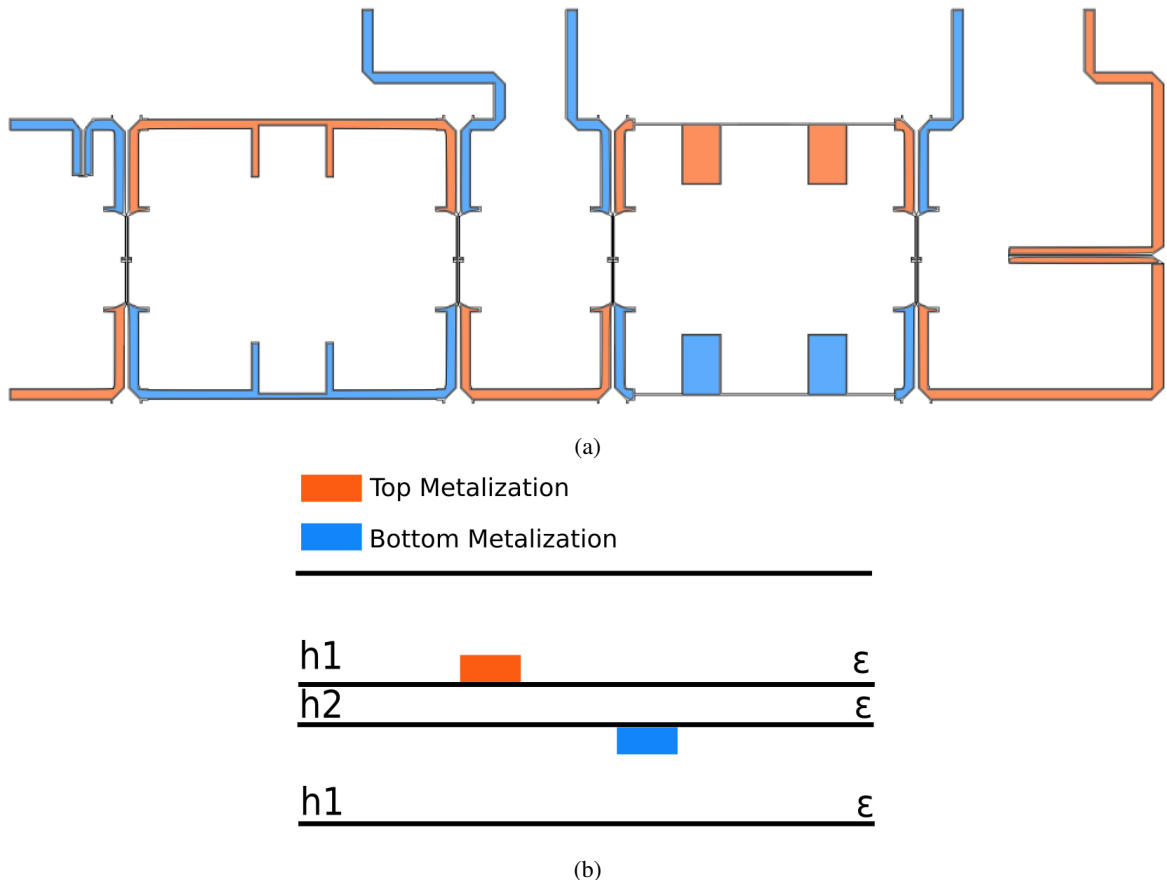


Fig. 4.8. Layout of the designed directional filter (a) and schematic cross-sectional view of the utilized stripline structure (b).

The designed directional filter was manufactured and measured. The simulated and measured scattering parameters of the directional filter are presented in Fig. 4.9. As seen the measurements confirm the electromagnetic simulations of the directional filter in terms of both magnitude and phase characteristics. The obtained phase difference between the outputs is acceptable even though it can be minimized with the use of circuits that are more complex to manufacture. However, AF calculations conducted for the measured characteristics of the directional filter showed that the HPBW variation will not exceed $\pm 2^\circ$ and the sidelobe level will not rise above -10 dB. Moreover, a more deteriorative effect is expected from the unavoidable coupling between the adjacent radiating elements. Therefore, such a directional filter is more than sufficient to be utilized in the feeding network of the two-octave scalable antenna array.

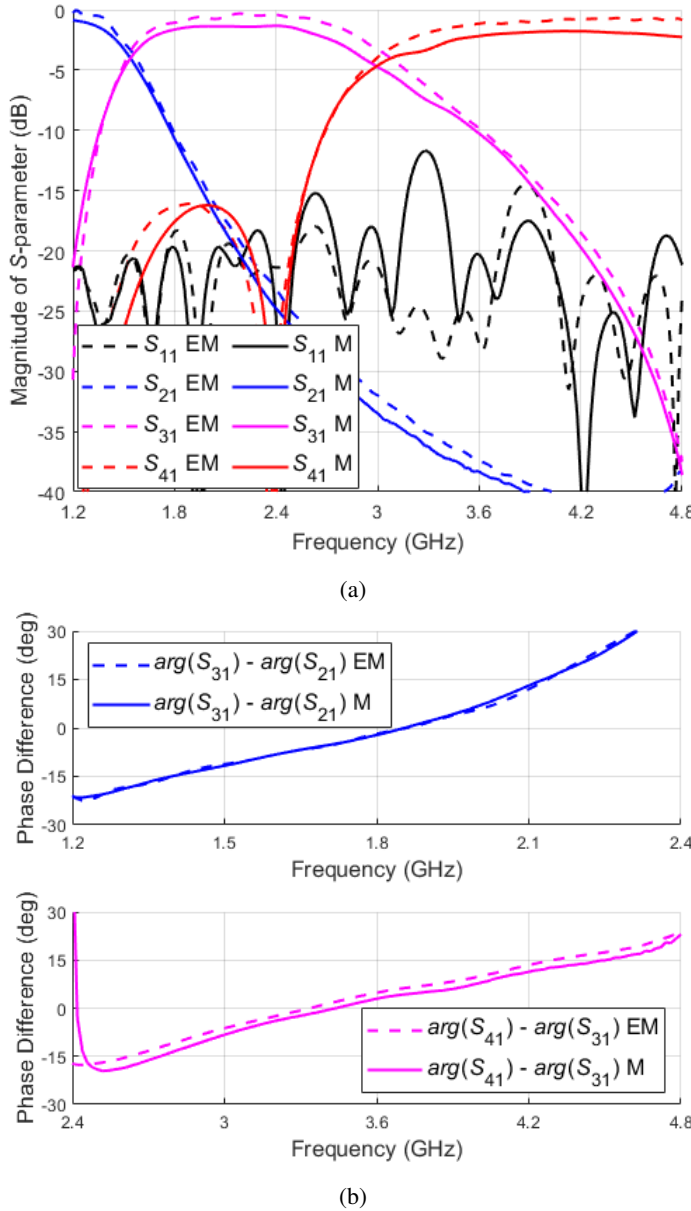


Fig. 4.9. Electromagnetically simulated and measured magnitude (a) and phase difference (b) characteristics of the manufactured directional filter.

4.3. Power dividers

The concept of the scalable antenna array, which utilizes a switching function between antenna subarrays, needs additional signal distribution between radiating elements if the amount of radiating elements is greater than one in each subarray. The developed antenna array operates in the two-octave frequency range and consists of three subarrays, each composed of four radiating elements. From this, it follows that the signal from each directional filter output should be distributed among the four antennas. All power dividers are composed of three broadband two-section Wilkinson power dividers, which distribute the signal from outputs of the directional filter to radiating elements in each subarray. Due to well-known

broadband impedance match techniques, which could be applied to the Wilkinson power divider, broadband structures are preferred instead of individual structures for each subband. Moreover, the Wilkinson power divider providing good performance in bandwidth 4:1 is relatively easy to design, and the feeding network does not need additional phase correction circuits, which would be required if power dividers were designed for subbands.

For the development, a microstrip structure where chosen. AD450 substrate that has dielectric constant equal to 4.4 with a thickness 0.76 mm has been used. In the proposed design, the characteristic impedance of the first section and second section is equal to 84.4Ω and 60.5Ω , respectively. The center frequency has been determined as $f_0 = 3.8 \text{ GHz}$. The length of each section selected in quarter wavelength at f_0 has been selected as $\ell = \frac{\lambda}{4} = 11 \text{ mm}$. In order to prevent the length of the design to take up a large space, each section has been bent in half circle shape. The transmission lines which connect the Wilkinson power divider and connectors have been designed as 50Ω lines having quarter wavelength at f_0 . However, each length of transmission line that connect the first two-section with the following two have been determined as $\frac{\lambda_H}{4}$ (f_H equal to 4.8 GHz). In the design process, the length of the lines between the power divider and connectors was modified to obtain a better impedance matching. Moreover, in the input stage of the divider, two groups of stubs were added. Stubs introduce additional capacitance connected to the ground in parallel, which improve impedance matching and shifts the divider's operating band to the lower frequencies. Utilization of curved transmission lines and additional stubs allowed for the miniaturization of the power divider. The resistors in the single two-section Wilkinson have been calculated with odd-even analysis, wherein in the odd mode, the input has been short-circuited, and in the even mode calculation, each resistor between sections becomes an open-circuit. Ultimate values of resistors have been determined in the optimization process when three broadband two-section Wilkinson power dividers were connected together. Electrical parameters of designed power divider have been presented in Fig. 4.2 and layout in Fig. 4.10.

The performance of the designed 4-Way Wilkinson power divider has been presented in Fig. 4.11. There are small differences between measurement and simulation results. These differences may be caused by losses in the printed circuit board measurement setup and due to the failure to take into account the influence of SMA connectors that introduce additional inductive reactance.

TABLE 4.2. Electrical parameters of the developed 4-Way Wilkinson power divider.

Parameter	Electrical value	Physical value
w_1	51.8Ω	1.35 mm
l_1	85.14°	10.23
w_2	84.4Ω	0.5 mm
l_2	90.05°	10.82 mm
w_3	60.5Ω	1.022 mm
l_3	90.4°	11 mm
l_c	71.35°	8.55 mm
l_f	113.2°	13.6 mm
w_s	—	0.25 mm
l_{s1}	—	1 mm
l_{s2}	—	1.5 mm

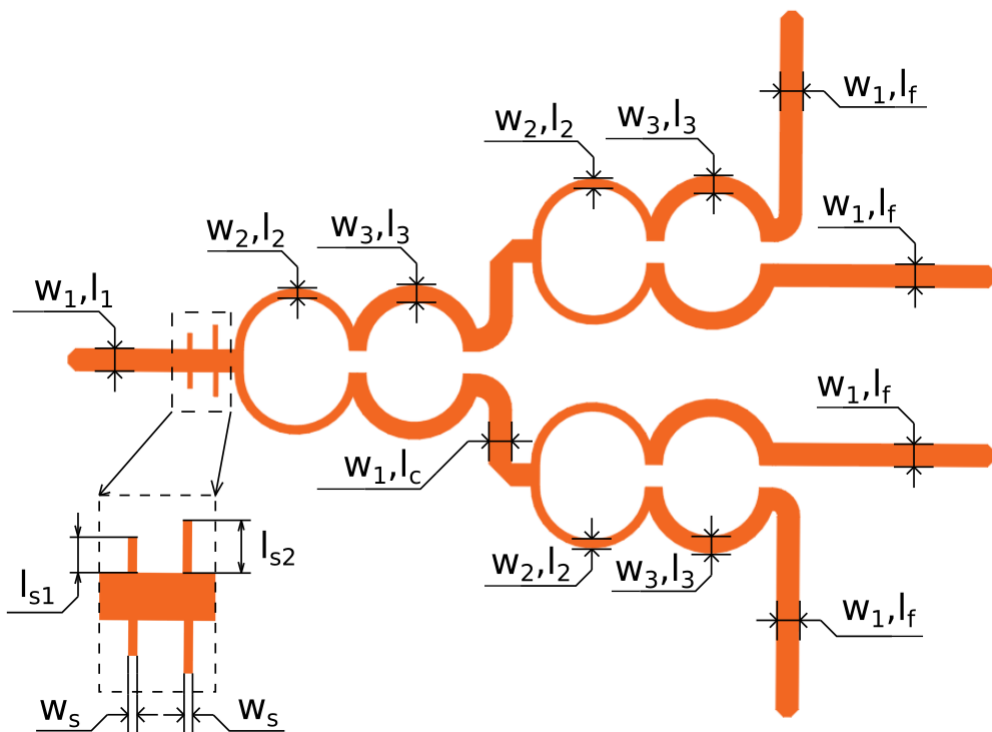


Fig. 4.10. Layout of designed 4-Way Wilkinson power divider.

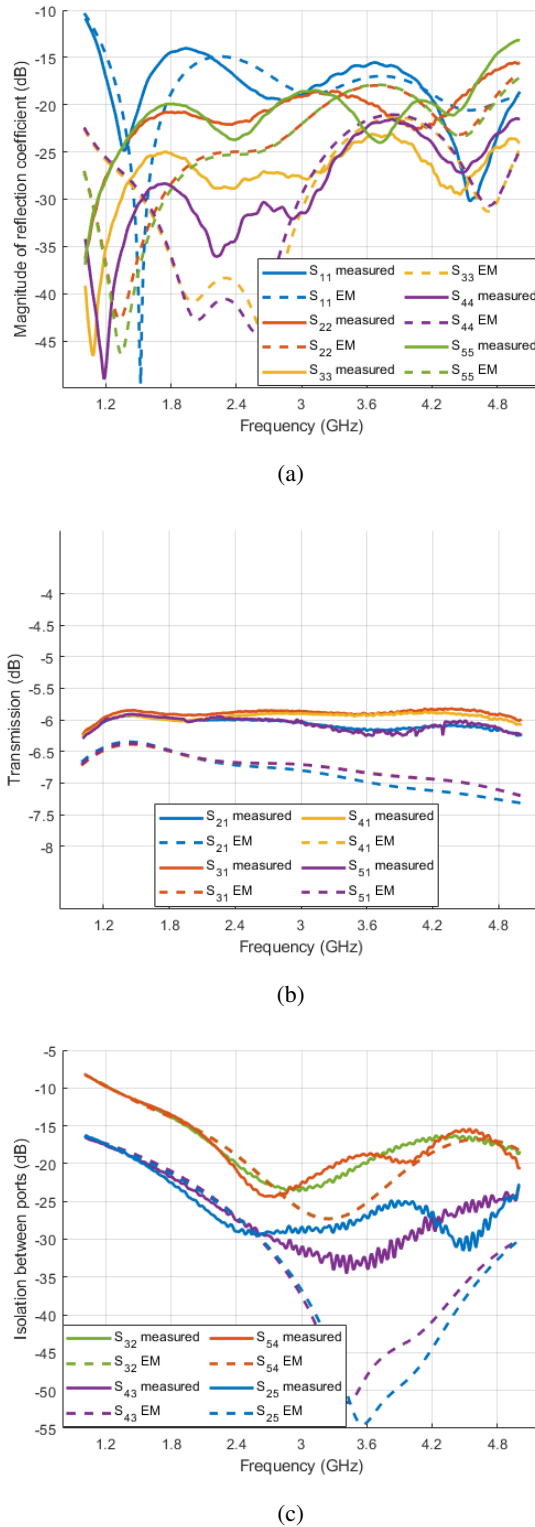


Fig. 4.11. Electromagnetically simulated and measured magnitude of return loss (a), transmission (b) isolation (c) of manufactured 4-Way Wilkinson power divider.

4.4. Radiating elements

As seen in Fig. 4.6, the developed scalable antenna array is composed of three centered subarrays. According to the concept, different radiating elements were utilized in each subarray. The subarrays fed from the LF and MF outputs are composed of linearly tapered slot antennas (LTSA) and the one fed from the HF output is composed of antipodal Vivaldi antennas. Such radiating elements were selected since they meet the theoretical requirements i.e., they feature stable radiation pattern and BW greater than one frequency octave. Moreover, all radiating elements feature end-fire radiation pattern that allows for their placement in the calculated positions. The designed radiating elements were manufactured and measured. For antipodal Vivaldi antennas dielectric laminate, having dielectric constant equal to 3.38 and thickness equal to 0.79 mm was utilized. On the other hand, the LTSA antennas were manufactured with the use of a dielectric laminate having dielectric constant and thickness equal to 4.4 and 0.6 mm, respectively. Fig. 4.12 presents the layouts of the LTSA and antipodal Vivaldi, whereas the physical dimensions of all the antennas are shown in Tables 4.3, 4.4, and 4.5. Measured reflection coefficients of the utilized antenna elements are shown in Fig. 4.13. As seen each radiating element features a good impedance match (S_{11} below -10 dB) in a different part of the operational frequency range from 1.2 GHz to 4.8 GHz. For each antenna element radiation patterns were measured. These measurements were conducted for ten discrete frequencies that were uniformly spaced across the subbands in which the radiating element operates and features a good impedance match. The results are shown in Fig. 4.14. As seen all of the elements feature an acceptable HPBW variation across the required BW which allows for their utilization in the developed antenna array.

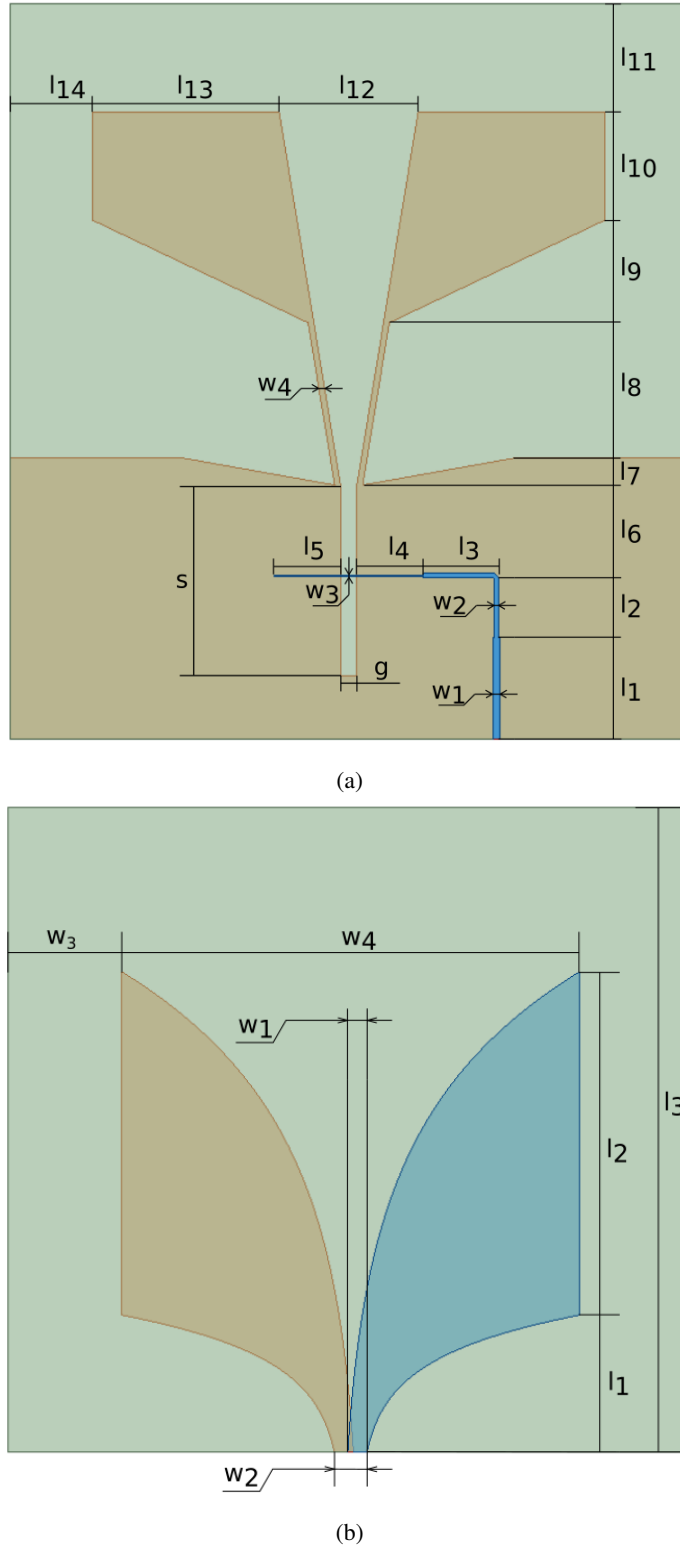


Fig. 4.12. Layouts of the LTSA (a) and antipodal Vivaldi (b).

TABLE 4.3. Dimensions of the developed LF LTSA.

Parameter	Value
l_1	17.6 mm
l_2	10.4 mm
l_3	12.33 mm
l_4	11.61 mm
l_5	11.63 mm
l_6	15.38 mm
l_7	4.82 mm
l_8	23.42 mm
l_9	17.83 mm
l_{10}	18.75 mm
l_{11}	19 mm
l_{12}	24.17 mm
l_{13}	32.92 mm
l_{14}	14.42 mm
g	2.8 mm
s	33 mm
w_1	1.2 mm
w_2	0.8 mm
w_3	0.3 mm
w_4	1 mm

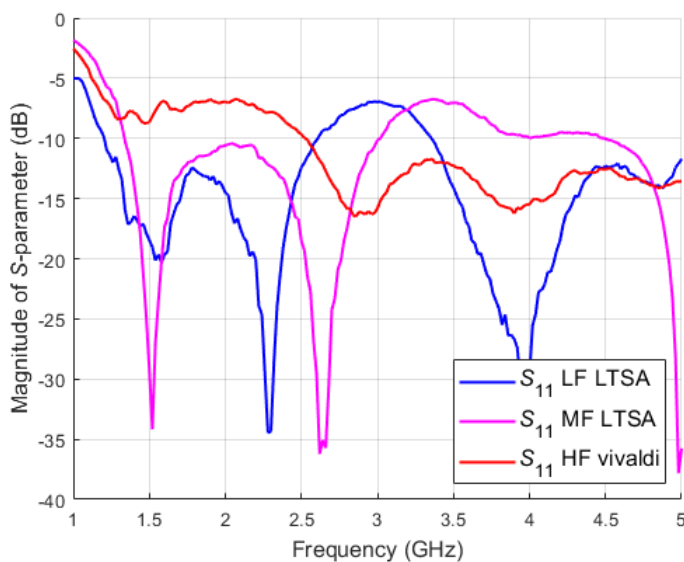
**Fig. 4.13.** Measured reflection coefficient of the developed antenna elements.

TABLE 4.4. Dimensions of the developed MF LTSA.

Parameter	Value
l_1	19.8 mm
l_2	8.55 mm
l_3	8.55 mm
l_4	5.64 mm
l_5	10.24 mm
l_6	15.03 mm
l_7	4.82 mm
l_8	23.38 mm
l_9	17.87 mm
l_{10}	18.75 mm
l_{11}	19 mm
l_{12}	24.17 mm
l_{13}	32.5 mm
l_{14}	14.42 mm
g	2.52 mm
s	31.6 mm
w_1	1.2 mm
w_2	0.8 mm
w_3	0.3 mm
w_4	1 mm

TABLE 4.5. Dimensions of the developed HF antipodal Vivaldi.

Parameter	Value
l_1	14.43 mm
l_2	36.34 mm
l_3	68.2 mm
w_1	2 mm
w_2	3.5 mm
w_3	10.3 mm
w_4	51.3 mm

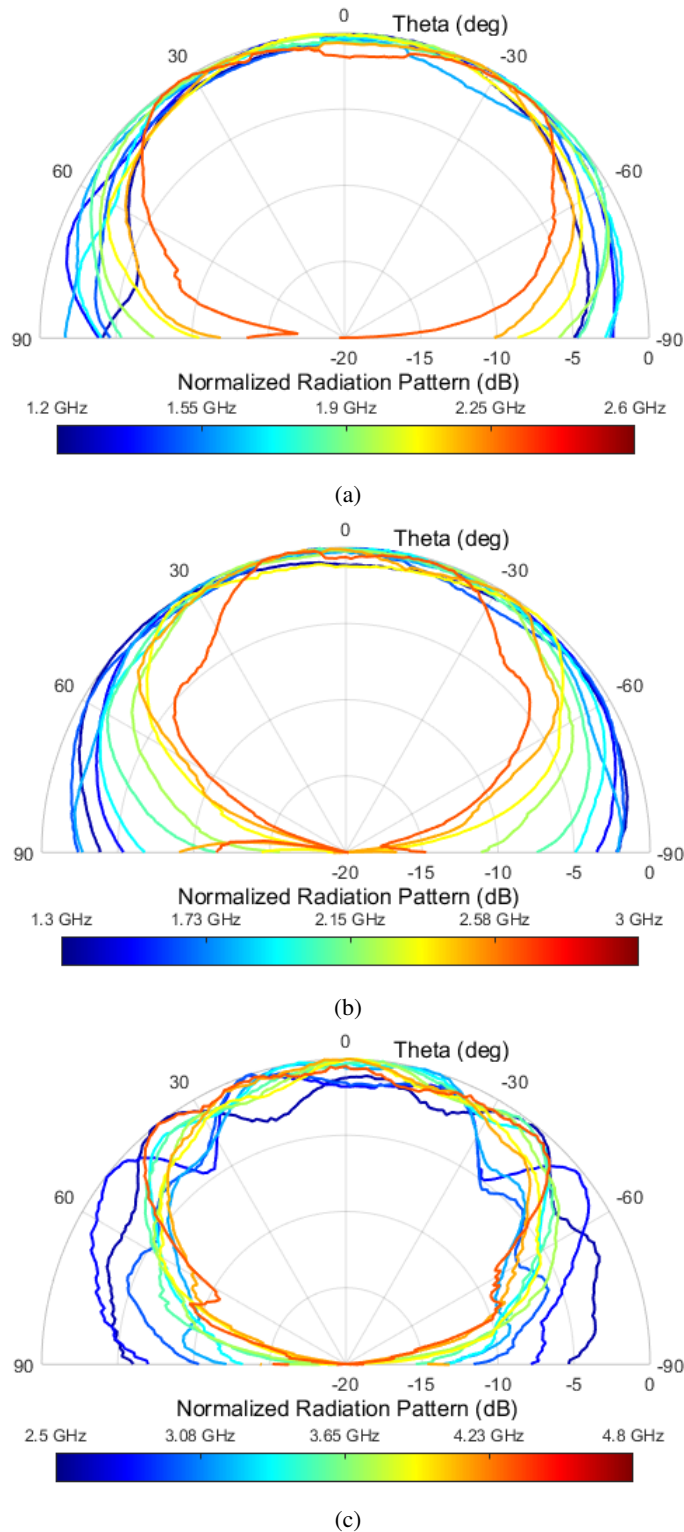


Fig. 4.14. Measured radiation patterns of LF LTSA (a), MF LTSA (b), and HF antipodal Vivaldi (c). Radiation patterns were measured in the subbands of operation.

4.5. Measured results

The developed scalable antenna array and feeding network were assembled and placed on a robotic arm in an anechoic chamber as seen in Fig. 4.15. The radiation pattern of the antenna array was measured for ten discrete frequencies that were uniformly spaced across the 1.2 – 4.8 GHz frequency range. The measured results are presented in Fig. 4.16. As seen the antenna array features a stable radiation pattern across the two-octave frequency range. The resulting HPBW variation does not exceed $\pm 4.5^\circ$ and the beam direction variation is not greater than $\pm 1^\circ$. A discrepancy in the measured sidelobe level compared to the calculated one is observed. This discrepancy is a result of the couplings between the adjacent radiating elements. These couplings can be reduced by utilization of radiation elements having different geometries as seen in the presented approach. Utilization of only LTSA radiating elements for all of the subarrays would cause the increase of the inter-element coupling, and therefore result in a malfunctioning scalable antenna array. However, the obtained results are acceptable since the radiation pattern is stable and the sidelobe level is below -5 dB. The conducted measurements confirm the correctness of the presented concept of multi octave scalable antenna arrays. Therefore, such an approach can be utilized to design and manufacture scalable antenna arrays operating in multi octave frequency range. Moreover, this concept can be utilized to develop not only broadside beam scalable antenna arrays, but also to develop multibeam scalable antenna arrays. To implement multibeam antennas, a feeding network should be properly adjusted by addition of the same directional filters and circuitis responsible for phase progression between the group of elements.

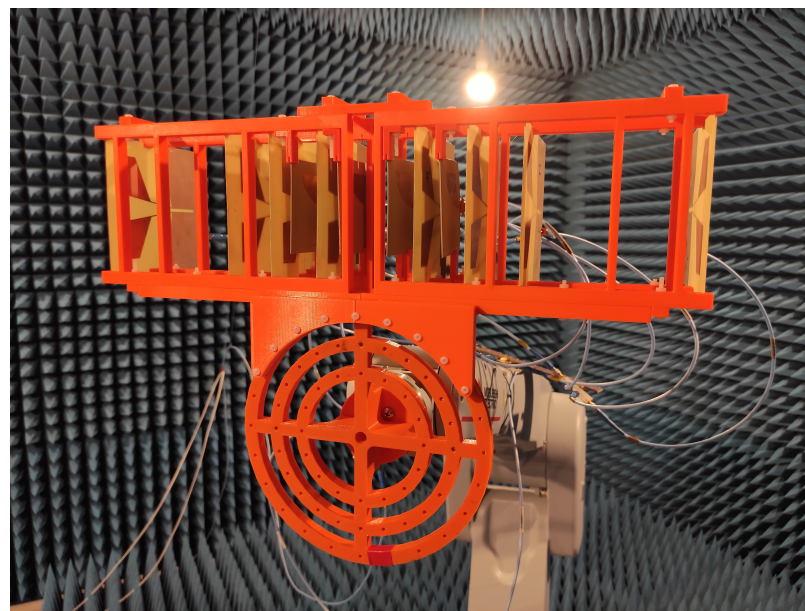


Fig. 4.15. The assembled scalable antenna array with the feeding network in an anechoic chamber.

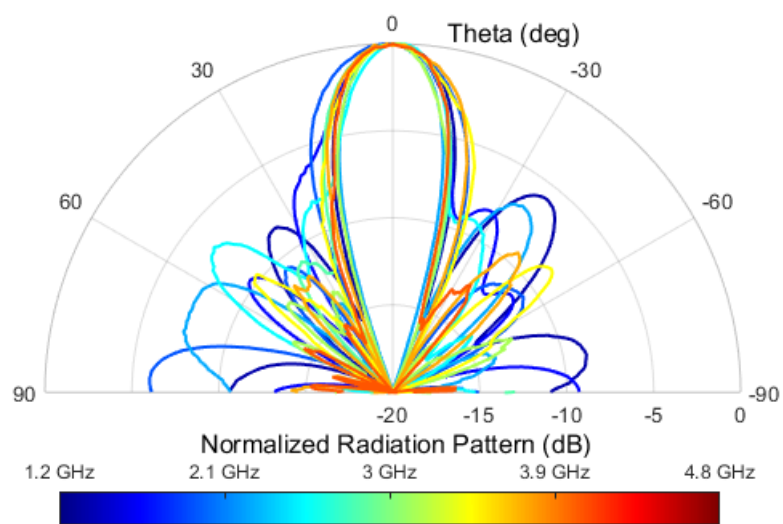


Fig. 4.16. Measured radiation pattern of the developed scalable antenna array.

5. Conclusions

This thesis was based on research regarding scalable antenna arrays that was conducted by the authors and presented in [15], [16], [17], and [18]. Firstly, the theory of antenna arrays, the principle of scalable antenna arrays' operation, and two methods for theoretical analysis were shown in Chapter 2. One of the methods i.e., the method of virtual radiating element was developed by one of the authors. Both methods were utilized to theoretically analyze scalable antenna arrays that feature both multibeam and broadside beam radiation patterns. In Chapter 3, five concepts of multibeam scalable antenna arrays were presented, whereas a concept of a broadside beam scalable antenna array that can be scaled in terms of bandwidth and number of radiating elements is discussed in Chapter 4. All the developed concepts were verified experimentally. For that reason, scalable antenna arrays, composed of radiating elements and appropriate feeding networks, were designed, manufactured, and measured. The measurements confirm the correctness of all scalable antenna arrays' concepts.

The authors want to emphasize that the further research regarding scalable antenna arrays is needed since that field of antenna array's technology has not been fully explored. Therefore, authors want to indicate two aspects on which the future research can be focused. First, the feeding networks utilized in scalable antenna arrays can be improved and minimized. Moreover, novel feeding networks e.g., active ones, can be explored since in our research of scalable antenna arrays only passive feeding networks have been utilized. The second aspect that can be explored is the reduction of the coupling between radiating elements in the antenna array. Minimization or reduction of the inter-element coupling would improve the overall performance of the scalable antenna arrays since this effect has the most disruptive influence on the achieved radiation pattern.

Bibliography

- [1] Constantine A. Balanis. “Antenna Theory: Analysis and Design”. In: 4th ed. Hoboken: John Wiley & Sons, Inc., 2016. Chap. 9.
- [2] Hao Wang, Shu-Fang Liu, Lei Chen, Wen-Tao Li, and Xiao-Wei Shi. “Gain enhancement for broadband vertical planar printed antenna with H-shaped resonator structures”. In: *IEEE Transactions on Antennas and Propagation* 62.8 (2014), pp. 4411–4415. DOI: [10.1109/TAP.2014.2325955](https://doi.org/10.1109/TAP.2014.2325955).
- [3] Kai-Ran Xiang, Fu-Chang Chen, Qing-Xin Chu, and Michael J. Lancaster. “A broadband 3×4 Butler matrix and its application in multibeam antenna arrays”. In: *IEEE Transactions on Antennas and Propagation* 67.12 (2019), pp. 7622–7627. DOI: [10.1109/TAP.2019.2934793](https://doi.org/10.1109/TAP.2019.2934793).
- [4] Krzysztof Wincza and Slawomir Gruszczyński. “Broadband integrated 8×8 Butler matrix utilizing quadrature couplers and Schiffman phase shifters for multibeam antennas with broadside beam”. In: *IEEE Transactions on Microwave Theory and Techniques* 64.8 (2016), pp. 2596–2604. DOI: [10.1109/TMTT.2016.2582877](https://doi.org/10.1109/TMTT.2016.2582877).
- [5] Constantine A. Balanis. “Antenna Theory: Analysis and Design”. In: 4th ed. Hoboken: John Wiley & Sons, Inc., 2016. Chap. 6.
- [6] Kai-Ran Xiang and Fu-Chang Chen. “ 4×4 broadband Butler matrix and its application in antenna arrays”. In: *2019 IEEE International Symposium on Antennas and Propagation and USNC-URSI Radio Science Meeting*. 2019, pp. 675–676. DOI: [10.1109/APUSNCURSINRSM.2019.8889133](https://doi.org/10.1109/APUSNCURSINRSM.2019.8889133).
- [7] Krzysztof Wincza, Kamil Staszek, Izabela Slomian, and Slawomir Gruszczyński. “Scalable multi-beam antenna arrays fed by dual-band modified Butler matrices”. In: *IEEE Transactions on Antennas and Propagation* 64.4 (2016), pp. 1287–1297. DOI: [10.1109/TAP.2016.2521888](https://doi.org/10.1109/TAP.2016.2521888).
- [8] Krzysztof Wincza and Slawomir Gruszczyński. “Broadband scalable antenna arrays with constant beamwidths fed by frequency-selective networks”. In: *IEEE Transactions on Antennas and Propagation* 64.7 (2016), pp. 2936–2943. DOI: [10.1109/TAP.2016.2560959](https://doi.org/10.1109/TAP.2016.2560959).
- [9] Krzysztof Wincza and Slawomir Gruszczyński. “Frequency-selective feeding network based on directional filter for constant-beamwidth scalable antenna arrays”. In: *IEEE Transactions on Antennas and Propagation* 65.8 (2017), pp. 4346–4350. DOI: [10.1109/TAP.2017.2717962](https://doi.org/10.1109/TAP.2017.2717962).

- [10] Dakotah J. Simpson and Dimitra Psychogiou. “Frequency-dependent feeding methods for broadband Vivaldi arrays with minimum half-power beamwidth (HPBW) variation”. In: *IEEE Open Journal of Antennas and Propagation* 2 (2021), pp. 564–577. DOI: [10.1109/OJAP2021.3075418](https://doi.org/10.1109/OJAP2021.3075418).
- [11] Dakotah J. Simpson and Dimitra Psychogiou. “Broadband monopole array with reduced half-power beamwidth variation”. In: *IEEE Access* 9 (2021), pp. 128454–128459. DOI: [10.1109/ACCESS.2021.3111822](https://doi.org/10.1109/ACCESS.2021.3111822).
- [12] Krzysztof Wincza, Kamil Staszek, and Sławomir Gruszczyński. “Broadband multibeam antenna arrays fed by frequency-dependent Butler matrices”. In: *IEEE Transactions on Antennas and Propagation* 65.9 (2017), pp. 4539–4547. DOI: [10.1109/TAP.2017.2722823](https://doi.org/10.1109/TAP.2017.2722823).
- [13] Kamil Staszek, Szczepan Odrobina, Krzysztof Wincza, and Sławomir Gruszczyński. “Broadband matrix-type feeding networks for two-beam antennas with constant beamwidth and efficient aperture utilization”. In: *Journal of Electromagnetic Waves and Applications* 33.2 (2019), pp. 236–248. DOI: [10.1080/09205071.2018.1536565](https://doi.org/10.1080/09205071.2018.1536565).
- [14] Kamil Staszek, Sławomir Gruszczyński, and Krzysztof Wincza. “Broadband feeding networks based on directional filters for two-beam antenna arrays”. In: *Journal of Electromagnetic Waves and Applications* 34.9 (2020), pp. 1300–1307. DOI: [10.1080/09205071.2019.1657964](https://doi.org/10.1080/09205071.2019.1657964).
- [15] Andrzej Dudek, Piotr Kanios, Kamil Staszek, Sławomir Gruszczyński, and Krzysztof Wincza. “Octave-band four-beam antenna arrays with stable beam direction fed by broadband 4×4 butler matrix”. In: *Electronics* 10.21 (2021), p. 2712. DOI: [10.3390/electronics10212712](https://doi.org/10.3390/electronics10212712).
- [16] Andrzej Dudek, Piotr Kanios, Sławomir Gruszczyński, and Krzysztof Wincza. “Octave-band three-beam antenna array with broadside beam fed by broadband Butler matrix”. In: *USNC-URSI Radio Sci. Meeting, Joint AP-S Symp.* 2022, submitted, accepted.
- [17] Andrzej Dudek, Piotr Kanios, Krzysztof Wincza, and Sławomir Gruszczyński. “Octave-band three-beam scalable antenna array fed by broadband 4×4 Butler matrix”. In: *MIKON-2022 Conf.* 2022, submitted, under review.
- [18] Andrzej Dudek, Piotr Kanios, Kamil Staszek, Sławomir Gruszczyński, and Krzysztof Wincza. “Scalable antenna arrays featuring stable radiation pattern in multi octave bandwidth”. In: *IEEE Transactions on Antennas and Propagation* (2022), submitted, under review.
- [19] Hang Zhao Chen Lin Fan Zhang Fu-Shun Zhang and Yong-Chnag Jiao. “A loaded wideband linearly tapered slot antenna with broad beamwidth”. In: *IEEE Antennas and Wireless Propagation Letter* 10 (2011), pp. 79–82. DOI: [10.1109/LAWP.2011.2106477](https://doi.org/10.1109/LAWP.2011.2106477).
- [20] Sławomir Gruszczyński and Krzysztof Wincza. “Broadband 4×4 Butler matrices as a connection of symmetrical multisection coupled-line 3-dB directional couplers and phase correction networks”. In: *IEEE Transactions on Microwave Theory and Techniques* 57.1 (2009), pp. 1–9. DOI: [10.1109/TMTT.2008.2009081](https://doi.org/10.1109/TMTT.2008.2009081).

- [21] Sławomir Gruszczyński, Krzysztof Wincza, and Krzysztof Sachse. “Broadband 4×4 Butler matrices utilizing tapered-coupled-line directional couplers”. In: *2011 MICROWAVES, RADAR AND REMOTE SENSING SYMPOSIUM*. 2011, pp. 77–81. DOI: [10.1109/MRRS.2011.6053605](https://doi.org/10.1109/MRRS.2011.6053605).
- [22] Sławomir Gruszczyński and Krzysztof Wincza. “Design of high-performance broadband multi-section symmetrical 3-DB directional couplers”. In: *Microwave and Optical Technology Letters* 50.3 (2008), pp. 636–638. DOI: <https://doi.org/10.1002/mop.23169>.